arXiv:1412.8243v2 [astro-ph.SR] 4 Mar 2015

High Dispersion Spectroscopy of Solar-type Superflare Stars.
I. Temperature, Surface Gravity, Metallicity, and $v \sin i$

Yuta Notsu[1], Satoshi Honda[2], Hiroyuki Maehara[3,4], Shota Notsu[1], Takuya Shibayama[5], Daisaku Nogami[1,6], and Kazunari Shibata[6]

ynotsu@kwasan.kyoto-u.ac.jp

[1]*Department of Astronomy, Kyoto University, Kitashirakawa-Oiwake-cho, Sakyo-ku, Kyoto 606-8502*

[2]*Center for Astronomy, University of Hyogo, 407-2, Nishigaichi, Sayo-cho, Sayo, Hyogo 679-5313*

[3]*Kiso Observatory, Institute of Astronomy, School of Science, The University of Tokyo, 10762-30, Mitake, Kiso-machi, Kiso-gun, Nagano 397-0101*

[4]*Okayama Astrophysical Observatory, National Astronomical Observatory of Japan, 3037-5 Honjo, Kamogata, Asakuchi, Okayama 719-0232*

[5]*Solar-Terrestrial Environment Laboratory, Nagoya University, Furo-cho, Chikusa-ku, Nagoya, Aichi, 464-8601*

[6]*Kwasan and Hida Observatories, Kyoto University, Yamashina-ku, Kyoto 607-8471*

(Received 29-Sep-2014; accepted 26-Dec-2014)

Abstract

We conducted high dispersion spectroscopic observations of 50 superflare stars with Subaru/HDS, and measured the stellar parameters of them. These 50 targets were selected from the solar-type (G-type main sequence) superflare stars that we had discovered from the Kepler photometric data. As a result of these spectroscopic observations, we found that more than half (34 stars) of our 50 targets have no evidence of binary system. We then estimated effective temperature ($T_{\rm eff}$), surface gravity ($\log g$), metallicity ([Fe/H]), and projected rotational velocity ($v \sin i$) of these 34 superflare stars on the basis of our spectroscopic data. The accuracy of our estimations is higher than that of Kepler Input Catalog (KIC) values, and the differences between our values and KIC values ($(\Delta T_{\rm eff})_{\rm rms} \sim 219$K, $(\Delta \log g)_{\rm rms} \sim 0.37$ dex, and $(\Delta[{\rm Fe/H}])_{\rm rms} \sim 0.46$ dex) are comparable to the large uncertainties and systematic differences of KIC values reported by the previous researches. We confirmed that the estimated $T_{\rm eff}$ and $\log g$ values of the 34 superflare stars are roughly in the range of solar-type stars. In particular, these parameters and the brightness variation period (P_0) of 9 stars are in the range of "Sun-like" stars ($5600 \leq T_{\rm eff} \leq 6000$K, $\log g \geq 4.0$, and $P_0 > 10$ days). Five of the 34 target stars are fast rotators ($v \sin i \geq 10$km s^{-1}), while

22 stars have relatively low $v \sin i$ values ($v \sin i < 5$km s^{-1}). These results suggest that stars whose spectroscopic properties similar to the Sun can have superflares, and this supports the hypothesis that the Sun might cause a superflare.

Key words: stars: flare — stars: solar-type —stars: rotation — stars: activity — stars:abundances

1. Introduction

Flares are energetic explosions in the stellar atmosphere and are thought to occur by impulsive releases of magnetic energy stored around starspots, like solar flares (e.g., Shibata & Magara 2011). The total energy released in the largest solar flares is estimated to be of the order of 10^{32}erg (e.g., Priest 1981; Emslie et al. 2012). Many T Tau stars, RS CVn-type binary stars, and dMe stars have "superflares," which have a total energy of $\sim 10^{33-38}$ erg (Schaefer et al. 2000), 10-10^6 times larger than that of the largest solar flares on the Sun. Such stars generally rotate fast ($P_{\rm rot}$ ∼a few days and $v \sin i \gtrsim$10km s^{-1}) and magnetic fields of a few kG are considered to be distributed in large regions on the stellar surface (Gershberg 2005; Shibata & Yokoyama 1999, 2002). In contrast, the Sun slowly rotates ($P_{\rm rot}$ ∼25 days and $v \sin i$ ∼2km s^{-1}), and the mean magnetic field is weak (a few G). It had been thought that superflares cannot occur on slowly-rotating G-type main-sequence stars like the Sun before our recent discoveries using Kepler described in the following, except for the report by Schaefer et al. (2000).

We recently have analyzed the data obtained with the Kepler space telescope (Koch et al. 2010), and discovered 365 superflare events on 148 solar-type (G-type main-sequence) stars from the data of 83,000 solar-type stars for the first 120 days of the Kepler mission (Maehara et al. 2012). We here define "*solar-type stars*" as stars that have a surface temperature of $5100 \leq T_{\rm eff} \leq 6000$K and a surface gravity of $\log g \geq 4.0$. Then, we extended the study of Maehara et al. (2012), and found 1547 superflare events on 279 solar-type stars by using Kepler data of a longer period (∼500 days) (Shibayama et al. 2013). Kepler is very useful for detecting small increases in the stellar brightness caused by stellar flares, because Kepler realized high photometric precision exceeding 0.01% for moderately bright stars, and obtained continuous time-series data of many stars over a long period (Koch et al. 2010). Kepler data have also been used for stellar flare research on M and K-type stars (Walkowicz et al. 2011; Candelaresi et al. 2014) and on A and F-type stars (Balona 2012).

The analyses of Kepler data enabled us to discuss statistical properties of superflares since a large number of flare events were discovered. Before the discoveries by Kepler, only

9 flare candidates of superflares on solar-type (G-type main sequence) stars were reported by Schaefer et al. (2000)[1], and the number of discovered events were too few to discuss statistical properties. Shibayama et al. (2013) confirmed that the occurrence rate (dN/dE) of the superflare versus the flare energy (E) shows a power-law distribution of $dN/dE \propto E^{-\alpha}$, where $\alpha \sim 2$, and that this distribution is roughly similar to that for the solar flare. Shibayama et al. (2013) also estimated that a superflare with an energy of 10^{34-35}erg occurs once in 800-5000 years in Sun-like stars. "*Sun-like stars*" are here defined as solar-type stars with an effective temperature of $5600 \leq T_{\rm eff} \leq 6000$K, a surface gravity of $\log g \geq 4.0$, and a rotation period (P) longer than 10 days.

Many of superflare stars show quasi-periodic brightness variations with a typical period of from one day to a few tens of days. The amplitude of these brightness variations is in the range of 0.1-10% (Maehara et al. 2012), and is much more larger than that of solar brightness variation (0.01-0.1%; e.g., Lanza et al. 2003) caused by the existence of sunspots on the rotating solar surface. Notsu et al. (2013b) showed that these brightness variations of superflare stars can be well explained by the rotation of a star with fairly large starspots, taking into account the effects of the inclination angle and the spot latitude. Notsu et al. (2013b) also clarified that the superflare energy is related to the total coverage of the starspot, and that the superflare energy can be explained by the magnetic energy stored around these large starspots. In addition, Shibata et al. (2013) suggested, on the basis of theoretical estimates, that the Sun can generate large magnetic flux that is sufficient for causing superflares with an energy of 10^{34} erg within one solar cycle ($\sim$11yr). The results of the superflare researches are becoming extremely important in many fields, for example, magnetic activity research in solar/stellar physics (e.g., Aulanier et al. 2013; Shibata et al. 2013; Candelaresi et al. 2014) and planetary habitability in astrobiology (e.g., Segura et al. 2010).

The results described above are, however, only based on Kepler monochromatic photometric data. We need to spectroscopically investigate whether these brightness variations are explained by the rotation, and whether superflare stars have large starspots. The stellar parameters and the binarity of the superflare stars are also needed to be investigated by spectroscopic observations, in order to discuss whether the Sun can really generate superflares. We have already reported the first results of our spectroscopic observations of three superflare stars in Notsu et al. (2013a) and Nogami et al. (2014). Notsu et al. (2013a) confirmed that one superflare star KIC6934317 is a G-type main-sequence star. We investigated its chromospheric activity by using Ca II infrared triplet and Hα lines, and these lines of this star suggest high chromospheric activity. We also measured the projected rotational velocity ($v \sin i$) of this star, and confirmed that this star has a small inclination angle by comparing $v \sin i$ with the period

[1] Some of these 9 events seem doubtful as summarized in Footnote 1 of Nogami et al. (2014).

of the brightness variation. Nogami et al. (2014) found that spectroscopic properties ($T_{\rm eff}$, $\log g$, [Fe/H], and rotational velocity) of the two superflare stars KIC9766237 and KIC9944137 are very close to those of the Sun. This supports the hypothesis that the Sun can cause a superflare. Apart from our previous spectroscopic studies (Notsu et al. 2013a and Nogami et al. 2014), Wichmann et al. (2014) performed spectroscopic observations of 11 superflare stars, and found several stars of them are young, fast-rotating stars where high levels of stellar activity can be expected. For the remaining stars, however, they said that they did not find a straightforward explanation for the occurrence of superflares.

We have then performed high-dispersion spectroscopy of more superflares stars (50 stars in total). In this paper, we first describe the details of these observations, and judge whether the target stars are single or binary stars. We then estimate the effective temperature ($T_{\rm eff}$), surface gravity ($\log g$), metallicity ([Fe/H]), and projected rotational velocity ($v \sin i$) of our target stars. On the basis of stellar parameters derived in this paper (Paper I), we investigate whether the quasi-periodic brightness variation observed by Kepler is explained by the rotation, and whether superflare stars have large starspots in Notsu et al. (2015; hereinafter Paper II). Ca II infrared triplet and Hα lines, which we have already used for investigating chromospheric activity of three superflare stars in Notsu et al. (2013a) and Nogami et al. (2014), are also analyzed in Paper II.

We describe the selection of the target stars and the details of our observation in Section 2. We discuss the binarity of the targets in Section 3.1. In Section 3.2$\sim$3.4, we then estimate stellar parameters ($T_{\rm eff}$, $\log g$, [Fe/H], $v \sin i$, and stellar radius $R_{\rm s}$) of the target stars. Finally in Section 4, we comment on the binarity and estimated stellar parameters of superflare stars, and then perform some analyses in order to check whether these spectroscopically derived values are good sources to discuss the actual properties of stars in our next papers (e.g., Paper II).

2. Targets and Observation

2.1. Target stars

We selected 50 superflare stars as target stars. The names of these 50 stars and their stellar parameters are listed in Table 1. Lightcurves of these 50 stars are shown in Supplementary Figure 1. Forty-six of these 50 stars were solar-type superflare stars reported in Shibayama et al. (2013). The way that we selected these 46 solar-type superflare stars as targets is summarized in the following. First, we listed all the *solar-type stars* ($5100 \leq T_{\rm eff,KIC} \leq 6000$K

and $(\log g)_{\rm KIC} \geq 4.0$) having superflare events reported in Shibayama et al. (2013). They are 279 stars in total. We then rejected relatively faint stars ($K_p > 14.5$mag) from the list of the target stars since the target stars should be bright enough to conduct Subaru/HDS observations with reasonable exposure time. We finally selected the 46 stars that have 3 following features with higher priority as target stars. (1) The brightness variation period reported in Shibayama et al. (2013) is relatively long ($P_{\rm S} > 10$ days). (2) The temperature is similar to the Sun ($5600 \leq T_{\rm eff,KIC} \leq 6000$K). (3) The brightness variation amplitude of the star, which is listed in Online Table of Shibayama et al. (2013), is relatively large ($\gtrsim$0.1%). We used the criteria (1) and (2), since we decided to choose stars that are relatively similar to the Sun, among the superflare stars we had already discovered. We used the criteria (3) since such stars are expected to have large starspots. There was no clear order of priority among the criteria (1), (2), and (3).

In addition to the above 46 solar-type superflare stars, we also observed the other 4 superflare stars (KIC6934317, KIC7420545, KIC8429280, and KIC11560431). These 4 superflare stars were not included in Shibayama et al. (2013), since they are not classified as solar-type stars on the basis of Kepler Input Catalog (KIC; Brown et al. 2011). We newly confirmed that these 4 stars are also superflare stars by using the same flare detection method reported in Maehara et al. (2012) and Shibayama et al. (2013). KIC6934317 is a G-type sub-giant star ($(\log g)_{\rm KIC} \sim 3.8$) on the basis of KIC data, and we have already reported the observational results of this star in Notsu et al. (2013a), as mentioned in Section 1. KIC7420545 is a K-type sub-giant star ($(\log g)_{\rm KIC} \sim 3.8$), and KIC8429280 and KIC11560431 are K-type main sequence stars, respectively, on the basis of KIC. We observed these three stars (KIC7420545, KIC8429280 and KIC11560431) since they are relatively bright ($K_p \lesssim 10$ mag) among the superflare stars that we had discovered by using Kepler data. Adding up these 4 stars and the above 46 solar-type superflare stars, we observed 50 superflare stars in total in this observation. In addition, five of the 50 target stars can be identified with the ROSAT X-ray all-sky survey source (Voges et al. 1999; Voges et al. 2000). We listed these five stars in Table 2.

Shibayama et al. (2013) and Notsu et al. (2013b) analyzed the Kepler data [2] of Quarter 0$\sim$6

[2] As discussed in García et al. (2011), the analyses of Kepler data needs the pre-processing of the data in order to correct the instrumental perturbations (e.g., outliers, jumps and drifts). We then already used the Kepler data detrended by the PDC-MAP pipeline (Stumpe et al. 2012) in Shibayama et al. (2013) and Notsu et al. (2013b). Through this, many errors such as outliers and temperature drifts are expected to be corrected. In addition to this, we already conducted the following correction in Shibayama et al. (2013) and Notsu et al. (2013b) in order to correct the sudden changes (jumps) in the mean values of the lightcurve at the "gaps" of the data (e.g., data gaps between the quarters). In this correction process, we calculated the mean flux values of each group of continuous data points between the gaps in the lightcurve, and adjusted the flux values of each data group so that the above mean value became equal to each other. We also removed a linear trend of the data in each quarter. We applied the above pre-processing processes of the Kepler data to the data that

(∼500 days), and estimated the period of the brightness variation ($P_{\rm S}$) that are listed in both Table 1 and Supplementary Table 1. As described in Section 2 of Notsu et al. (2013b), this variation period ($P_{\rm S}$) was calculated by choosing the peak from the Fourier power spectrum whose amplitude had the highest ratio to the red noise spectrum (e.g., Press 1978; Vaughan 2005). The power spectra used for estimating $P_{\rm S}$, which are calculated from the Kepler data of Quarter 0∼6 (∼500 days), are shown in Supplementary Figure 1. In this paper, we newly estimate the brightness variation period (P_1) by using the Kepler data of Quarter 2∼16 (∼1500 days) [3]. We did not use the Kepler data of the remaining three quarters (Q0, Q1, and Q17) since the data period of these three quarter is short ($\lesssim$ 30 days) compared to those of the other 15 quarters (∼90 days) (Thompson et al. 2013d), and we consider that long-term variations (P ∼30 days) cannot well be detected by using the data of these three quarters. The method of estimating this new period value (P_1) is the same as that we used in Shibayama et al. (2013) and Notsu et al. (2013b). The power spectra used for calculating P_1 are also shown in Supplementary Figure 1. We also estimated other period values P_2 and P_3, which correspond to the second and third peak of the power spectra used for estimating P_1, respectively. The estimated values of P_1, P_2 and P_3 are listed in Supplementary Table 1.

We compared these period values ($P_{\rm S}$, P_1, P_2 and P_3) in Appendix 1 (Figure 11 (a) and Supplementary Table 1), and checked the lightcurves and power spectra by eye shown in Supplementary Figure 1. We then selected the resultant period value P_0 from P_1, P_2 and P_3. The selection method consists of the following two steps. First, we exclude P_1, P_2 and P_3 value with low signal-to-noize ratio (S/N<25). Next, we select one appropriate period value (P_0) from P_1, P_2 and P_3 with S/N≥25 by checking the lightcurve and power spectrum of each star by eye. In this eye-check process, we confirmed whether the periodicity corresponding to the peak having the highest S/N ratio in the power spectrum are also clearly seen in the lightcurve. The P_0 values are also listed in Supplementary Table 1 and plotted in Figure 11 (b). In many cases, P_1 is adopted as P_0. In the following, we use only P_0 as the period of the brightness variation. It is because P_0 is estimated from the longer term data (∼ 1500 days) than $P_{\rm S}$ (∼ 500 days), and some irregular trends, such as effects of starspot evolution and disappearance, are expected to be averaged to some extent.

---

were newly analyzed in the following of this paper.

[3] The version of Kepler data used for calculating P_1 are different from those used for $P_{\rm S}$ in Shibayama et al. (2013) and Notsu et al. (2013b) (cf. Table 1 of Notsu et al. 2013b). We used the latest version of each quarter (Q2∼Q16) data. Q2∼Q14 data that we used here were opened to the public in Data release 21 (Thompson et al. 2013b), Q15 data were in Data release 20 (Thompson et al. 2013a), and Q16 data were in Data release 22 (Thompson et al. 2013c), respectively.

2.2. Details of Observations and Data Reduction

Our spectroscopic observations were carried out by using the High Dispersion Spectrograph (HDS: Noguchi et al. 2002) attached at the 8.2-m Subaru telescope during the semester S11B (2011 August 3), S12B (2012 August 6, 7, 8 and September 22, 23, 24, 25), and S13A (2013 June 23, 24). The spectral coverage was about 6100∼8820Å. This range includes the chromospheric-activity sensitive lines of Hα 6563Å and Ca II infrared triplet 8498, 8542, 8662Å. The 2×2 on-chip binning mode was adopted. Spectroscopic resolution ($R = \lambda/\Delta\lambda$) of each observation date is as follows; $R \sim 100,000$ in S11B (slit width of 0".36), $R \sim 51,000$ in S12B (slit width of 0".7), and $R \sim 80,000$ in S13A (slit width of 0".45). We used image slicer #2 (Tajitsu et al. 2012)[4] in S13A observation. Data reduction (bias subtraction, flat fielding, aperture determination, scattered light subtraction, spectral extraction, wavelength calibration, normalization by the continuum, and heliocentric radial velocity correction) was conducted using the ECHELLE package of the IRAF[5] software.

The observation date of each target star, exposure time of each observation, and obtained signal-to-noise ratio (S/N) are shown in Supplementary Table 2. We observed 50 superflare stars as mentioned above, and 19 stars were observed multiple times. In addition to these 50 superflare stars, we observed 10 bright solar-type stars and the Moon as references of solar-type (G-type main sequence) stars. These 10 stars are relatively bright ($V < 8.5$ mag) and easily observable during our observation period with Subaru/HDS, considering the coordinates of them. Among these 10 comparison stars, 8 stars (18 Sco, HD163441, HD173071, HIP100963, HIP71813, HIP76114, HIP77718, and HIP78399) are reported as "solar-twin" stars by the previous studies (King et al. 2005; Takeda & Tajitsu 2009; Datson et al. 2012). Stellar parameters of these stars are estimated in detail by these previous studies. In Appendix 3, we compare these parameters of the previous studies with those derived by us in this paper, and check whether our result of spectroscopic determination of stellar parameters is consistent with that of the previous studies, especially for the stars whose spectrum is similar to the solar one. In addition to the above 8 "solar-twin" stars, we observed two bright solar-type stars 59 Vir and 61 Vir. These two stars are first used for the above comparison process in Appendix 3, as the above 8 "solar-twin" stars are done. We also use these two stars as comparison stars in the discussion of stellar chromospheric activity in Paper II, as we have already used in Notsu et al. (2013a). 59 Vir rotates fast and has the strong average magnetic field (∼500 G), while 61 Vir rotates slowly and no magnetic field is detected (Anderson et al. 2010). In addition to the above 10 comparison stars, the Moon was

[4] Information of Image Slicers is summarized at http://www.naoj.org/Observing/Instruments/HDS/is.html

[5] IRAF is distributed by the National Optical Astronomy Observatories, which is operated by the Association of Universities for Research in Astronomy, Inc., under cooperate agreement with the National Science Foundation.

also observed as a comparison star whose spectrum is quite similar to the solar one in this observation, as done in many previous studies (e.g., Takeda & Tajitsu 2009; Takeda et al. 2010).

The Kepler lightcurves obtained around the periods of S11B and S12B observations are shown in Figure 13 in Appendix 2. There are no lightcurve data for S13A observation since Kepler ended its general observation mode on 2013 May (Thompson et al. 2013d). No flare events were detected during the observation time.

3. Analyses and Results

3.1. Binarity

For the first step of our analyses, we checked the binarity of each superflare star. First, we examined slit viewer images of Subaru/HDS of our target stars, and DSS (Space Telescope Science Institute Digital Sky Survey) images of them. Four stars (KIC4138557, KIC4750938, KIC5896387, and KIC11560431) have visual companion stars as shown in Figure 1. These four visual binary stars have "yes (VB)" in the 2nd column of Table 1. Although it is not clear whether these "visual" companion stars are real binary components of our target stars, we did not obtain spectra of them because of the following two reasons: (1) we cannot avoid contaminations of the visual companion star in the spectrum of the targets, and (2) we cannot distinguish which star generated superflares in the Kepler data [6].

Second, we investigated the line profiles, and found that 9 stars (KIC4045215, KIC5445334, KIC7264976, KIC8479655, KIC9653110, KIC9764192, KIC9764489, KIC10120296, and KIC10453475) have double-lined profiles. In this process, we checked by eye the profile of the main spectral lines (Hα 6563, Ca II 8542, and 4 Fe I lines in the range of 6212-6220Å) that are shown in Supplementary Figure 2. We also checked by eye the profile of other many ($\sim$50-100) Fe I and II lines of the stars that are not classified as binary stars in this paper, simultaneously with measuring equivalent width values of these lines in Section 3.2. The double-lined spectra of KIC4045215 and KIC7264976 are shown in Figure 2 (a) as examples. Figures of all the stars that are considered spectroscopic binary stars are available in Supplementary Figure 2. Since these double-lined profiles are caused by overlap of the radiation of multiple stars, we regard these 9 stars as double-lined spectroscopic binary stars. These 9 stars have "yes (SB2)" in the 2nd column of Tables 1.

[6] The pixel scale of the Kepler CCDs is about 4 arcsec and the typical photometric aperture for a 12 mag star contains about 30 pixels (van Cleve & Caldwell 2009).

Third, we investigated time variations of the line profiles between multiple observations that are expected to be caused by the orbital motion in the binary system. This investigation was for the target stars that we observed multiple times (16 stars). We measured the radial velocity (RV) of all the target stars that were not classified as visual binary stars or double-lined spectroscopic binary stars [7]. We used Fe I & II lines for measuring RV values. The estimated RVs and the numbers of lines we used here are listed in Supplementary Table 2. The errors of RVs listed in Supplementary Table 2 are the standard deviations of the RV values that are calculated for individual lines. As a result, KIC7902097 shows a large RV change (> 70km s^{-1}) as shown in Figure 2 (b). We consider that this star is in a binary system, and this star has "yes (RV)" in the 2nd column of Table 1. Moreover, the shapes of Hα line profile of KIC8226464 and KIC11073910 have large variations between the multiple observations as shown in Figure 2 (b), though RV values of the main component does not vary significantly. We here consider that these variations result from the orbital motion in the binary system, and that KIC8226464 and KIC11073910 are also spectroscopic binary stars. These stars have "yes (Hα-vari)" in the 2nd column of Table 1.

In total, we regard 16 superflare stars as binary stars, as summarized in Table 3 [8]. The remaining 34 superflare stars does not show any evidence of binarity within the limits of our analyses, so we treat them as "single stars" in this paper. These stars have "no" in the 2nd column of Tables 1. In the following section, we conduct the detailed analyses only for these 34 stars.

Spectra of photospheric lines, including Fe I 6212, 6215, 6216, 6219, of the 34 "single" superflare stars, 10 comparison stars, and Moon are shown in Figure 3. We observed 13 superflare stars multiple times among these 34 superflare stars. Three comparison stars (59 Vir, 61 Vir, and 18 Sco) are also observed multiple times. We made co-added spectra of these 16 stars by conducting the following two steps. First, we shifted the wavelength value of each spectrum to the laboratory frame on the basis of the radial velocity value of each observation. These radial velocity values are listed in Supplementary Table 2. Next, we added up these shifted spectra to one co-added spectrum. These co-added spectra are mentioned as "S12B-comb" or "S13A-comb" in Supplementary Table 2. In Figures 3, co-added spectra of these 16 stars are used. Only the co-added spectra are used in the following sections of this paper when we analyze the spectral data of these 16 stars that we observed multiple times.

[7] We do not measure the radial velocities of each component of the double-lined profiles of these stars in this paper, since it is not necessary for the following discussions in this paper.

[8] The binary stars are also divided into sub-groups of different period of the brightness variation in Table 3. This classification of binary stars is just for reference in order to confirm how many stars with the brightness variation period as long as that of the Sun ($P \gtrsim 20$ days) are included among all our target stars.

3.2. Temperature, Surface Gravity, and Metallicity

We estimate the effective temperature $T_{\rm eff}$, surface gravity $\log g$, microturbulence $v_{\rm t}$, and metallicity [Fe/H] of the 34 single superflare stars 10 comparison stars, and Moon (Sun), by measuring the equivalent widths of Fe I and Fe II lines. The method is basically the same as the one we used in Notsu et al. (2013a) and Nogami et al. (2014), which is originally based on Takeda et al. (2002, 2005). We summarize the method in the following.

We used Fe I and Fe II lines in the range of $6120 - 8370$Å, selected from the line list presented in Online Data of Takeda et al. (2005). In the process of measuring equivalent widths, we used the code SPSHOW contained in SPTOOL software package[9] developed by Y. Takeda, which was originally based on Kurucz's ATLAS9/WIDTH9 model atmospheric programs (Kurucz 1993). For deriving $T_{\rm eff}$, $\log g$, $v_{\rm t}$, and [Fe/H] from measured equivalent widths, we used TGVIT program[10] developed by Y. Takeda. The procedures adopted in this program are minutely described in Takeda et al. (2002) and Takeda et al. (2005).

The resultant atmospheric parameters ($T_{\rm eff}$, $\log g$, $v_{\rm t}$, and [Fe/H]) of the 34 single superflare stars, 10 comparison stars, and Moon (Sun) are listed in Tables 4 and 5, respectively (Table 5 is in Appendix 3.). The values of KIC6934317, KIC9766237, and KIC9944137 in Table 4 were already reported in our previous papers. We reported the values of KIC6934317 in Notsu et al. (2013a), and the values of KIC9766237 and KIC9944137 in Nogami et al. (2014). In Table 4, we adopt the atmospheric parameters of KIC8429280 reported by Frasca et al. (2011)[11] since the rotational velocity of KIC8429280 is so high and the spectral lines are too wide to estimate these atmospheric parameters. For the same reason, we use the atmospheric parameters of KIC9652680 reported by KIC.

In addition to Table 4, Figure 4 also shows our $T_{\rm eff}$, $\log g$, and [Fe/H] of the 34 single superflare stars. Equivalent width values of all lines of all the stars that we measured in the above process are also listed in Supplementary Data.

---

[9] http://optik2.mtk.nao.ac.jp/∼takeda/sptool/

[10] http://optik2.mtk.nao.ac.jp/∼takeda/tgv/

[11] Frasca et al. (2011) provides two sets of the atmospheric parameters: one derived with SYNTHE and the other derived with ROTFIT, which agree with each other within 1-sigma error bars. In this paper, we adopt the parameters derived with ROTFIT since they use the ROTFIT values in the process of estimating Li abundances, and we plan to refer to this value in our future paper.

3.3. Projected Rotational Velocity

We measure $v \sin i$ (stellar projected rotational velocity) of the target stars by using the method that is basically the same as in Notsu et al. (2013a) and Nogami et al. (2014). The method is originally based on the one described in Takeda et al. (2008). We summarize the method in the following.

We took into account the effects of macroturbulence and instrumental broadening on the basis of Takeda et al. (2008). According to Takeda et al. (2008), there is a simple relationship among the line-broadening parameters, which can be expressed as

$$v_{\rm M}^2 = v_{\rm ip}^2 + v_{\rm rt}^2 + v_{\rm mt}^2 \ . \tag{1}$$

Here, $v_{\rm M}$ is e-folding width of the Gaussian macrobroadening function $f(v) \propto \exp[-(v/v_{\rm M})^2]$, including instrumental broadening ($v_{\rm ip}$), rotation ($v_{\rm rt}$), and macroturbulence ($v_{\rm mt}$). We derived $v_{\rm M}$ by applying an automatic spectrum-fitting technique (e.g Takeda 1995a; Takeda et al. 2008), assuming the model atmosphere corresponding to the atmospheric parameters estimated in Section 3.2. In this process, we used the MPFIT program contained in the SPTOOL software package. Takeda et al. (2008) applied this fitting technique to 6080-6089Å region, and derived $v \sin i$ values by fitting spectral lines in this region simultaneously. We basically adopt their method, but, as we have already mentioned in Notsu et al. (2013a), this region is out of the spectral coverage of our observation (6100∼8820Å). Because of this, we applied the above fitting technique to 6212∼6220Å region, which we selected on the basis of the following reasons. First, this spectral range contains 4 Fe I lines shown in Figure 3, and we can fit these multiple lines simultaneously. Second, this range does not have so strong lines (Equivalent width values of the 4 Fe I lines are less than 100mÅ), and the continuum level is easy to be determined. Third, this range is expected to have relatively high S/N within the range of this observation (6100∼8820Å). Finally, we have already used this region in Notsu et al. (2013a) and Nogami et al. (2014), and we would like to keep consistency between the results of this paper and those of these papers.

The instrumental broadening velocity $v_{\rm ip}$ corresponds to e-folding width of the Gaussian instrumental broadening function. This was calculated by using the following relation (Takeda et al. 2008),

$$v_{\rm ip} = \frac{3 \times 10^5}{2R\sqrt{\ln 2}} \ , \tag{2}$$

where $R(=\lambda/\Delta\lambda)$ is the resolving power of the observation. The macroturbulence velocity $v_{\rm mt}$ was estimated by using the relation $v_{\rm mt} \sim 0.42\zeta_{\rm RT}$ (Takeda et al. 2008). The term $\zeta_{\rm RT}$ is the radial-tangential macroturbulence, and we roughly estimate $\zeta_{\rm RT}$ by using the relation reported in Valenti & Fischer (2005),

$$\zeta_{\rm RT} = \left(3.98 - \frac{T_{\rm eff} - 5770{\rm K}}{650{\rm K}}\right), \quad (3)$$

where $T_{\rm eff}$ is the effective temperature of stars. Valenti & Fischer (2005) derived the equation (3) by taking the glowerh boundary of the upper limit of $\zeta_{\rm RT}$ as a function of $T_{\rm eff}$. Using these equations, we derived $v_{\rm rt}$ (e-folding width of the Gaussian rotational broadening function), and finally $v \sin i$ by using the relation $v_{\rm rt} \sim 0.94 v \sin i$ (Gray 2005).

The resultant $v \sin i$ values of the 34 single superflare stars, 10 comparison stars, and Moon (Sun) are listed in Tables 4 and 5, respectively. As mentioned in Section 3.2, the $v \sin i$ values of KIC6934317, KIC9766237 and KIC9944137 in Table 4 were already reported in our previous papers (Notsu et al. 2013a; Nogami et al. 2014). In Table 4, we adopt the $v \sin i$ value of KIC8429280 reported by Frasca et al. (2011) since we also used the atmospheric parameters reported by them in Section 3.2. The $v \sin i$ value of KIC9652680 is calculated from atmospheric parameters in KIC since we used the atmospheric parameters in KIC in Section 3.2. In this process, we assume that microturbulence velocity ($v_{\rm t}$) of KIC9652680 is 1 km s^{-1} as a typical value of the solar-type stars (see Table 4).

Hirano et al. (2012, 2014) estimated the systematic uncertainty of $v \sin i$ by changing $\zeta_{\rm RT}$ by $\pm$15% from Equation (3) for cool stars ($T_{\rm eff} \leq$6100K), on the basis of observed distribution of $\zeta_{\rm RT}$ (See also Figure 3 in Valenti & Fischer 2005). They explained that the statistical errors in fitting each spectrum are generally smaller than the systematic errors arising from different values of $\zeta_{\rm RT}$. We then used this type of error values arising from $\zeta_{\rm RT}$ as errors of $v \sin i$ listed in Tables 4 and 5.

Recently, Doyle et al. (2014) estimated $v \sin i$ values from asteroseismic analysis of 28 main-sequence stars observed by Kepler, and infer macroturblence velocity of them on the basis of these $v \sin i$ values. Using these results, they then derived the following new equation between macroturblence velocity, $T_{\rm eff}$, and $\log g$:

$$\zeta_{\rm RT} = 3.21 + 2.33 \times 10^{-3}(T_{\rm eff} - 5777) + 2.00 \times 10^{-6}(T_{\rm eff} - 5777)^2 - 2.00(\log g - 4.44) \ . \quad (4)$$

Figure 4 of Doyle et al. (2014) shows that there are some differences ($\Delta\zeta_{\rm RT} \sim$1 km s^{-1}) between the $\zeta_{\rm RT}$ estimated by using Equation (3) and those by Equation (4). For comparison, we then derived the new $v \sin i$ value of our targets by using this new equation (Equation (4)) in stead of Equation (3), which we used for estimating the $v \sin i$ value in the above paragraphs. The resultant value is listed in Supplementary Table 3. The error value of this new $v \sin i$ is estimated from the errors of Equation (4) ($\Delta\zeta_{\rm RT} \sim$0.73 km s^{-1}) reported in Doyle et al. (2014). In Figure 5, we compare this new $v \sin i$ value estimated by using Equation (4) with the original $v \sin i$ value by Equation (3). As shown in this figure, the difference between these

two $v \sin i$ values is not so large (<1 km s^{-1}) for most of the target stars. We have already used the values with Equation (3) in our previous researches (Notsu et al. 2013a; Nogami et al. 2014). Because of these two things, in the following sections of this paper and Paper II, we only use the original $v \sin i$ value estimated in the above paragraphs using Equation (3). This value with Equation (3) is plotted in the horizontal axis of Figure 5 and listed in Tables 4 and 5.

3.4. Stellar Radius

Using the stellar atmospheric parameters ($T_{\rm eff}$, $\log g$, and [Fe/H]) estimated in Section 3.2, we roughly estimated the stellar age and stellar mass ($M_{\rm s}$) for the target stars by applying the PARSEC isochrones [12] in Bressan et al. (2012). In this process, we selected all the data points having possible sets of $T_{\rm eff}$, $\log g$, and [Fe/H] from the PARSEC isochrones, taking into account the error values of $T_{\rm eff}$ and $\log g$ ($\Delta T_{\rm eff}$ and $\Delta \log g$, respectively) shown in Tables 4 and 5. There were three stars (KIC8359398, KIC9766237, and KIC10252382) that have no suitable isochrones within their original error range of $T_{\rm eff}$ and $\log g$. For these three stars, we then took into account $2\Delta T_{\rm eff}$ and $2\Delta \log g$. We must note that the resultant values of these three stars can have relatively low accuracy.

For each selected data point, we estimated $R_{\rm s}$ from the $M_{\rm s}$ and $\log g$ of each data point by using

$$\frac{R_{\rm s}}{R_\odot} = \sqrt{\left(\frac{M_{\rm s}}{M_\odot}\right) \Big/ \left(\frac{g}{g_\odot}\right)} \ . \tag{5}$$

We then selected the maximum and minimum $R_{\rm s}$ values of each star and determined the $R_{\rm s}$ value of each target star as a median between these maximum and minimum values. These $R_{\rm s}$ values of the target superflare stars and comparison stars are listed in Tables 4 and 5, respectively. The error values of $R_{\rm s}$ in these tables correspond to the above maximum and minimum $R_{\rm s}$ values of each target star. The error values of $R_{\rm s}$ shown in Table 4 are $\lesssim$20% for most of the stars. In addition, values of stellar age on the basis of the above isochrone are shown in Figure 6.

[12] http://stev.oapd.inaf.it/cgi-bin/cmd

4. Discussion

4.1. Binarity

In Section 3.1, we described that more than half (34 stars) of 50 target superflare stars have no evidence of binary system. We need to remember here that we cannot completely exclude the possibility that some of these 34 "single" superflare stars have companions, only with our limited observations above. We performed multiple observations only for 13 stars among 34 "single" stars, while the remaining 21 stars were observed only at once, as shown in column 3 of Supplementary Table 2. Then, we cannot completely exclude the possibility of showing radial velocity shifts especially for these 21 stars. It is necessary to observe these target stars more repeatedly in order to exclude the possibility of having binary stars as much as possible. Moreover, we also cannot completely exclude the possibility that the above 34 "single" stars have other faint neighboring stars such as M-dwarfs, even if no double-lined profiles and no radial velocity shifts were confirmed in this paper. In the process of investigating whether the target stars have double-lined profiles in Section 3.1, we only checked by eye the profile of the main spectral lines [13] (Hα 6563, Ca II 8542 and 4 Fe I lines in the range of 6212-6220Å) that are shown in Supplementary Figure 2. This suggests that the classification of double-lined spectroscopic binary stars is not complete. More detailed analyses such as the cross-correlation of the target and the template spectrum are needed to detect the signature of binarity caused by the existence of faint companion stars. We must note this point, but we consider that such detailed analyses of binarity are not really necessary for the overall discussion of stellar properties of superflare stars in this paper. We then expect the future detailed observations and analyses.

As mentioned in Section 1, close binary stars such as RS CVn-type stars have been widely known as active flare stars, which maintain high rotation rate and high flare activity thanks to the tidal interaction between the primary and companion stars (e.g., Walter & Bowyer 1981). It is very important whether our superflare stars are such close binary stars or not, especially for considering that single stars like the Sun can really have superflares. The 34 superflare stars show no double-lined profile, as explained above. This suggests that many of these 34 stars have no companions whose mass is on the same order of that of the primary star. This is because if such companions exist, the bolometric intensity of them is comparable to that of the primary star, and double-lined profile is expected to be observed in many cases. In particular, 13 stars among these 34 stars show no radial velocity shifts between the multiple observations. It is then possible that many of them are not close binary stars, though more multiple observations are needed, as mentioned in the previous paragraph of this section.

[13] We also checked by eye the profile of other many (∼50-100) Fe I and II lines of the stars that are not classified as binary stars in the process of measuring atmospheric parameters in Section 3.2.

In addition, the absolute value of radial velocity of the two stars (KIC7354508 and KIC9459362) are relatively large ($>$ 100km s^{-1}) compared to the other stars, as listed in Supplementary Table 2. This suggests the two possibilities that these stars are close binary stars or high-velocity stars. We cannot decide which possibilities are right since we observed them only at once and we cannot investigate changes of radial velocities. In this paper, we then treat them as single stars.

4.2. Estimated Stellar Parameters

In Section 3.2, we estimated the atmospheric parameters ($T_{\rm eff}$, $\log g$, [Fe/H]) of the 34 superflare stars, which are considered as single stars in Section 3.1. According to Figure 4(a), the measured $T_{\rm eff}$ and $\log g$ values of the 34 superflare stars are in the range of 5000$\sim$6300K and 3.5$\sim$4.9, respectively. This means that the stellar parameters of these superflare stars are roughly in the range of solar-type (G-type main sequence stars) stars, though 6 stars with $\log g < 4.0$ are possibly sub-giant G-type stars. In particular, the temperature, surface gravity, and the brightness variation period (P_0) of 9 stars including two stars (KIC9766237 and KIC9944137) reported in Nogami et al. (2014) are in the range of "Sun-like" stars ($5600 \leq T_{\rm eff} \leq 6000$K, $\log g \geq$4.0, and $P_0 >$10 days). The metallicity ([Fe/H]) of these stars are not so different from solar one as we can see in Figure 4(b). The root-mean-square residual between [Fe/H] of the observed superflare stars and that of the Sun is $\sim$0.23. No clear "metal-rich" or "metal-poor" stars are included in our target stars, though metallicity of the two stars (KIC9459362 and KIC10252382) are a bit lower ([Fe/H]< -0.6) than that of the other stars. These two a bit "metal-poor" stars are plotted in Figure 6 by using triangle points, and this figure suggests the possibility that these two stars are not young, though the detailed discussion of stellar age is beyond the scope of this paper, as also mentioned in the next paragraph.

Age of the target stars can roughly estimated by Figure 6 on the basis of the isochrone values. Information of the stellar age is important since the stellar activity have deep relation with the stellar age (e.g., Soderblom et al. 1991), but the detailed discussion of the stellar age is beyond the scope of this paper. We also plan to discuss the Li abundances and whether our target superflare stars are quite young or not in our future paper (Honda et al. in preparation) since the Li abundance is known to provide quite loose constraints on the age of G-type stars (e.g., Soderblom et al. 1993; Sestito & Randich 2005).

There are four stars below all the plotted isochrones (100Myr, 1Gyr, and 10Gyr) in Figure 6. They are KIC8359398, KIC9652680, KIC10387363 and KIC11818740. The $\log g$

values of them may be slightly overestimated for ordinary G-type main sequence stars. Regarding KIC9652680, the log g value in KIC is used, as mentioned in Section 3.2, and can be not so accurate, as we discuss in Section 4.3. The S/N ratios of the other three stars are relatively low (S/N$\lesssim$40 around Hα 6563Å) among our target stars (see Supplementary Table 2). This can possibly increase the error values of $\log g$.

In Section 3.3, we measured the projected rotational velocity ($v \sin i$) of the 34 superflare stars, which are considered as single stars in Section 3.1. The distribution histogram of $v \sin i$ for these stars are shown in Figure 7. The data of 119 ordinary solar-type stars reported in Takeda et al. (2010) are also plotted in this figure for reference. We can roughly regard the data of Takeda et al. (2010) as a random sample of the ordinary solar-type stars, considering their target selection method explained in Takeda et al. (2007). Comparison of these data in Figure 7 suggests that $v \sin i$ of the observed superflare stars tends to be higher than the sample of ordinary solar-type stars, though we need to remember here that the group of the target stars of our spectroscopic observations is not a really random sample of superflare stars, as explained in Section 2.1. In particular, 5 of the 34 target stars have extremely high $v \sin i$ value ($v \sin i \geq 10$km s^{-1}). On the other hand, 22 of the 34 target superflare stars have low $v \sin i$ value ($v \sin i < 5$km s^{-1}), and our target superflare stars include stars rotating as slow as the Sun ($v \sin i \sim$2 km s^{-1}). In Paper II, we will compare this $v \sin i$ value with other stellar properties such as the brightness variation observed by Kepler.

Summarizing the above discussions in Section 4.1 and 4.2, more than half (34 stars) of 50 target superflare stars have no evidence of binary system, and stellar atmospheric parameters of these stars are basically in the range of ordinary solar-type (G-type main sequence) stars. Moreover, these 34 stars include stars rotating as slow as the Sun ($v \sin i \sim$2 km s^{-1}). These results suggest that stars whose spectroscopic properties similar to the Sun can have superflares, and this supports the hypothesis that the Sun might cause a superflare. This is consistent with the result of our previous paper Nogami et al. (2014), which found that the spectroscopic properties of two superflare stars KIC9766237 and KIC9944137 are very close to those of the Sun.

4.3. Comparison of Our Estimated Stellar Parameters with the Previous Values

In the following, we performed some analyses in order to check whether these spectroscopically derived values are good sources to discuss the actual properties of stars. First, in Appendix 3, we confirmed that our resultant atmospheric parameters and measured equivalent width values of comparison stars are comparable to the results of previous researches. We can

say that our result of spectroscopic determination of atmospheric parameters is consistent with that of the previous studies. In the following, we investigate whether these spectroscopically derived atmospheric parameters of the target superflare stars are comparable to the parameters estimated from previous photometric catalogs.

We compared $T_{\rm eff}$, $\log g$ and [Fe/H] with those reported in Kepler Input Catalog (KIC; Brown et al. 2011), and show the results in Figure 8. In this Figure, spectroscopically derived values does not seem in so good agreement with KIC values. Spectroscopic $T_{\rm eff}$ and [Fe/H] values tend to be a bit higher than those in KIC, while spectroscopic $\log g$ values seem to have much poor correlation with those in KIC. The root-mean-square residual between the atmospheric parameter values we estimated and those in KIC are $(\Delta T_{\rm eff})_{\rm rms} \sim 219$K, $(\Delta \log g)_{\rm rms} \sim 0.37$ dex, and $(\Delta[{\rm Fe/H}])_{\rm rms} \sim 0.46$ dex, respectively. However, this result is comparable to the large uncertainties and systematic differences in KIC parameters reported by the previous researches (e.g., Molenda-Żakowicz et al. 2010; Brown et al. 2011; Bruntt et al. 2012; Thygesen et al. 2012; Hirano et al. 2014). For example, Brown et al. (2011) reported relatively large uncertainties of the temperature and surface gravity in KIC ($\pm$200K for $T_{\rm eff}$ and 0.4 dex for $\log g$), and also pointed out that the reliability of the metallicity in KIC is especially poor. Bruntt et al. (2012) compared their spectroscopic values with KIC values, and reported that their spectroscopic $T_{\rm eff}$ and [Fe/H] values are systematically higher by 165K and 0.21 dex than the values in KIC, respectively. These tendencies are also shown in our Figure 8(a) and (c). Summarizing the above points, we have measured stellar atmospheric parameters more accurately compared to KIC values, and differences between our values and KIC values ($(\Delta T_{\rm eff})_{\rm rms} \sim 219$K, $(\Delta \log g)_{\rm rms} \sim 0.37$ dex, and $(\Delta[{\rm Fe/H}])_{\rm rms} \sim 0.46$ dex) are comparable to the large uncertainties and systematic differences in KIC values reported by the previous researches.

We also compare our temperature value with the other catalog values for reference. As we have already explained in detail in Section 3.1 of Notsu et al. (2013a), Pinsonneault et al. (2012) reported a catalog [14] of revised $T_{\rm eff}$ for stars in the Kepler Input Catalog (KIC; Brown et al. 2011). They used two methods ("SDSS method" and "IRFM method") on the basis of stellar color values, and derived two revised temperature values ($T_{\rm eff,SDSS}$ and $T_{\rm eff,IRFM}$), respectively. We should note that Pinsonneault et al. (2012) estimate $T_{\rm eff,SDSS}$ and $T_{\rm eff,IRFM}$ values with fixing [Fe/H] values at the mean value of KIC ([Fe/H]=-0.2), and the comparison here is rough discussion. The $T_{\rm eff,SDSS}$ and $T_{\rm eff,IRFM}$ values of the 34 single target stars are listed in Supplementary Table 4. Pinsonneault et al. (2012) argued that these revised temperature values are both about 200K higher than the values of $T_{\rm eff}$ in the KIC. In Figure 9, we plotted $T_{\rm eff,SDSS}$ and $T_{\rm eff,IRFM}$ as a function of our temperature values estimated with our spectroscopic data ($T_{\rm eff}$). The root-mean-square residual between our temperature value and the above

[14] This catalog is available at http://vizier.cfa.harvard.edu/viz-bin/VizieR?-source=J/ApJS/199/30 .

two revised temperature values ($T_{\rm eff,SDSS}$ and $T_{\rm eff,IRFM}$) are $\sim$177K and $\sim$211K, respectively. Comparing Figure 8 (a) and Figure 9, the values we derived spectroscopically ($T_{\rm eff}$) seem to be a bit more consistent with these revised temperature values ($T_{\rm eff,SDSS}$ and $T_{\rm eff,IRFM}$) than with the temperature values in KIC ($T_{\rm eff,KIC}$).

Wichmann et al. (2014) already reported atmospheric parameter values of 11 superflare stars on the basis of their spectroscopic data. Among these 11 stars, 6 stars correspond to 34 single superflare stars that we discuss in this paper. For reference, we compare their $T_{\rm eff}$, $\log g$, and $v \sin i$ values with the values that we estimated in this paper, and show the results in Figure 10. The errors of the values in Wichmann et al. (2014) is large, and there are large disagreements especially for $v \sin i$ values. We consider that this large error values are caused by the low S/N ratio of the observation data in Wichmann et al. (2014)[15], that our spectroscopically derived values are a bit more accurate compared to the values of Wichmann et al. (2014). In addition, in Wichmann et al. (2014), the macroturbulence velocity ($\zeta_{\rm RT}$) was set to 3.0 km s^{-1}, and temperature dependence of the macroturbulence velocity, which are evaluated in Equation (3) or (4) was not incorporated. This can also possibly cause some differences between their $v \sin i$ values and our values. Because of these things, we do not use the values in Wichmann et al. (2014) in Paper II.

On the basis of the discussions above, we can confirm that our spectroscopically derived values are better sources to discuss the actual properties of superflare stars compared to KIC values. We only use the values that we derived spectroscopically in this paper when we discuss stellar properties in Paper II. However, we need to remember that $v \sin i$ values estimated in Section 3.3 can be strongly affected by the way of estimating macroturbulence ($\zeta_{\rm RT}$ in Section 3.3). We assumed Equation (3) in this paper, but this equation is an only rough approximation. The effect of errors in macroturbulence is especially large for slowly-rotating stars ($v \sin i \lesssim 2-3$km s^{-1}), as we can see in Figure 5. In this figure, the difference between the two $v \sin i$ value, which originally comes from the difference in the estimation method of macroturbulence velocity is a bit larger especially in the range of $v \sin i \lesssim 2-3$km s^{-1}. More accurate estimation of macroturbulence is difficult (e.g., Takeda 1995b), and we think that this is beyond the scope of this paper. Because of this, we need to remember that the uncertainty of $v \sin i$ is large especially for slowly-rotating stars ($v \sin i \lesssim 2-3$km s^{-1}).

[15] The S/N ratio of the observation data in Wichmann et al. (2014) is 17-70 in the range of 5012-6432Å, which are used by them for determining stellar parameters.

The authors sincerely thank the anonymous referee for his/her very useful and constructive comments. This study is based on observational data collected with Subaru Telescope, which is operated by the National Astronomical Observatory of Japan. We are grateful to Dr. Akito Tajitsu and other staffs of the Subaru Telescope for making large contributions in carrying out our observations. We would also like to thank Dr. Yoichi Takeda for his many useful advices on the analysis of our Subaru/HDS data, and for his opening the TGVIT and SPTOOL programs into public. Kepler was selected as the tenth Discovery mission. Funding for this mission is provided by the NASA Science Mission Directorate. The Kepler data presented in this paper were obtained from the Multimission Archive at STScI. This work was supported by the Grant-in-Aids from the Ministry of Education, Culture, Sports, Science and Technology of Japan (No. 25287039, 26400231, and 26800096).

References

Ammler-von Eiff, M., & Reiners, A. 2012, A&A, 542, A116

Anderson, R. I., Reiners, A., Solanki, S. K. 2010, A&A, 522, A81

Aulanier, G., Démoulin, P., Schrijver, C. J., Janvier, M., Pariat, E., & Schmieder, B. 2013, A&A, 549, A66

Balona, L. A. 2012, MNRAS, 423, 3420

Bressan, A., Marigo, P., Girardi, L., Salasnich, B., Dal Cero, C., Rubele, S., & Nanni, A., 2012, MNRAS, 427, 127

Brown, T.M., Latham, D. W., Everett, M. E., & Esquerdo, G. A. 2011, ApJ, 142, 112

Bruntt, H., et al. 2012, MNRAS, 423, 122

Candelaresi, S., Hillier, A., Maehara, H., Brandenburg, A., & Shibata, K. 2014, ApJ, 792, 67

Datson, J., Flynn, C., & Portinari, L. 2012, MNRAS, 426, 484

Doyle, A. P., Davies, G. R., Smalley, B., Chaplin, W. J., & Elsworth, Y. 2014, MNRAS, 444, 3592

Emslie, et al., 2012, ApJ, 759, 71

Frasca, A., Fröhlich, H.-E., Bonanno, A., Catanzaro, G., Biazzo, K., & Molenda-Żakowicz, J. 2011, A&A, 532A, 81F

García, R. A., Hekker, S., Stello, D., et al. 2011, MNRAS, 414, L6

Gershberg, R. E. 2005, Solar-Type Activity in Main-Sequence Stars (Berlin: Springer)

Gray, D. F. 2005, The Observation and Analysis of Stellar Photospheres, 3rd ed. (Cambridge: Cambridge University Press)

Hirano, T., Sanchis-Ojeda, R., Takeda, Y., Narita, N., Winn, J. N., Taruya, A., & Suto, Y. 2012, ApJ, 756, 66

Hirano, T., Sanchis-Ojeda, R., Takeda, Y., Winn, J. N., Narita, N., & Takahashi, Y., H. 2014, ApJ, 783, 9

King, J. R., Boesgaard, A. M., & Schuler, S. C. 2005, AJ, 130, 2318

Koch, D. G., et al. 2010, ApJ, 713, L79
Kurucz, R. L. 1993, Kurucz CD-ROM No.13, Atlas 9 Stellar Atmosphere Programs and 2 Grid [16]
Lanza, A. F., Rodonò, M., Pagano, I., Barge, P., & Llebaria, A. 2003, A&A, 403, 1135
Maehara, H., et al. 2012 Nature, 485, 478
McQuillan, A., Mazeh, T., & Aigrain, S. 2014, ApJS, 211, 24
Molenda-Żakowicz, J., et al. 2010, Astronomische Nachrichten, 331, 981
Nielsen, M. B., Gizon, L., Schunker, H., & Karoff, C. 2013, A&A, 557, L10
Nogami, D., Notsu, Y., Honda, S., Maehara, H., Notsu, S., Shibayama, T., & Shibata, K. 2014, PASJ, 2014, 66, L4
Noguchi, K., et al. 2002, PASJ, 54, 855
Notsu, S., Honda, S., Notsu, Y., Nagao, T., Shibayama, T., Maehara, H., Nogami, D., & Shibata, K. 2013a, PASJ, 65, 112
Notsu, Y., et al. 2013b ApJ, 771, 127
Notsu, Y., Honda, S., Maehara, H., Notsu, S., Shibayama, T., Nogami, D., & Shibata, K. 2015, PASJ, in press, arXiv:1412.8245 (Paper II)
Pinsonneault, M. H., An, D., Molenda-Żakowicz, J., & Chaplin, W. J. 2012, ApJS, 199, 30 [Erratum: 2013, ApJS, 208, 12]
Press, W. H. 1978, Comments on Astrophysics, 7, 103
Priest, E. R. 1981, Solar Flare Magnetohydrodynamics (New York; Gordon and Breach Science Publishers)
Reinhold, T., Reiners, A., & Basri, G. 2013, A&A, 560, A4
Schaefer, B. E., King, J. R., & Deliyannis, C. P. 2000, ApJ, 529, 1026
Segura, A., Walkowicz, L., Meadows, V., Kasting, J., & Hawley, S., 2010, Astrobiology, 10, 751
Sestito, P., & Randich, S. 2005, A&A, 442, 615
Shibata, K., & Yokoyama, T. 1999, ApJ, 526, L49
Shibata, K., & Yokoyama, T. 2002, ApJ, 577, 422
Shibata, K., & Magara, T. 2011, Living Rev. Sol. Phys, 8, 6
Shibata, K., et al. 2013 PASJ, 65, 49
Shibayama, T., et al. 2013 ApJS, 209, 5
Soderblom, D. R., Duncan, D. K., & Johnson, D. R. H. 1991, ApJ, 375, 722
Soderblom, D. R., Jones, B. F., Balachandran, S., Stauffer, J. R., Duncan, D. K., Fedele, S. B., & Hudon, J. D. 1993, AJ, 106, 1059
Stumpe, M. C., Smith, J. C., Van Cleve, J. E., et al. 2012, PASP, 124, 985
Tajitsu, A., Aoki, W., & Yamamuro, T. 2012, PASJ, 64, 77
Takeda, Y. 1995, PASJ, 47, 287
Takeda, Y. 1995, PASJ, 47, 337
Takeda, Y., Honda, S., Kawanomoto, S., Ando, H., & Sakurai, T. 2010, A&A, 515, A93
Takeda, Y., Ohkubo, M., & Sadakane, K. 2002, PASJ, 54, 451
Takeda, Y., Ohkubo, M., Sato, B., Kambe, E., & Sadakane, K. 2005, PASJ, 57, 27 [Erratum: PASJ, 57, 415]

[16] Available at http://kurucz.harvard.edu/PROGRAMS.html .

Takeda, Y., Kawanomoto, S., Honda, S., Ando, H., & Sakurai, T. 2007, A&A, 468, 663
Takeda, Y., Sato, B., & Murata, D. 2008, PASJ, 60, 781
Takeda, Y., & Tajitsu, A. 2009, PASJ, 61, 471
Thompson, S. E., et al. 2013, Kepler Data Release 20 Notes (KSCI-19060-001)
Thompson, S. E., et al. 2013, Kepler Data Release 21 Notes (KSCI-19061-001)
Thompson, S. E., et al. 2013, Kepler Data Release 22 Notes (KSCI-19062-001)
Thompson, S. E., et al. 2013, Kepler Data Release 23 Notes (KSCI-19063-001)
Thygesen, A. O., et al. 2012, A&A, 543, A160
Valenti, J. A., & Fischer, D. A. 2005, ApJ, 159, 141
van Cleve, J. E., & Caldwell, D. A. 2009, Kepler Instrument Handbook, KSCI-19033
Vaughan, S. 2005, A&A, 431, 391
Voges, W., et al. 1999, A&A, 349, 389
Voges, W., et al. 2000, IAU Circ., 7432, 3
Walkowicz, L. M., et al. 2011, AJ, 141, 50
Walter, F. M., & Bowyer, S. 1981, ApJ, 245, 671
Wichmann, R., Fuhrmeister, B., Wolter, U., & Nagel, E. 2014, A&A, 567, A36

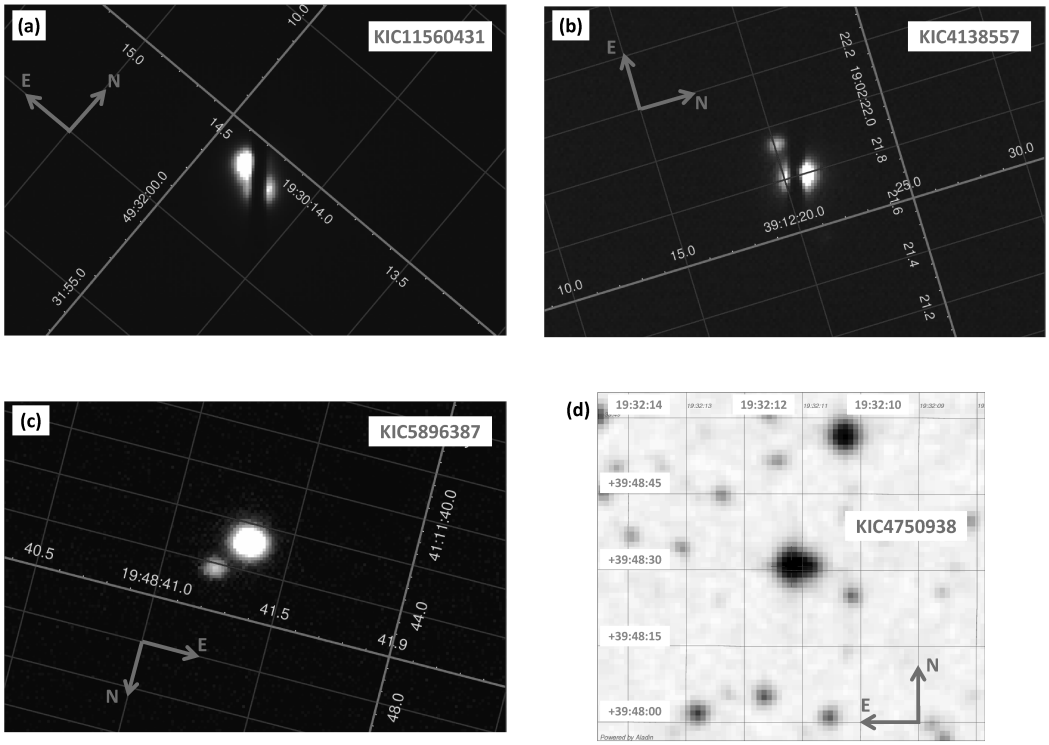

Fig. 1. (a), (b) and (c) : Slit viewer images of KIC11560431, KIC4138557, and KIC5896387, respectively. These stars were found to have visual companion stars by checking Slit Viewer images of Subaru/HDS. (d) DSS (Space Telescopes Science Institute Digital Sky Survey) image of KIC4750938. This figure also shows existence of a visual companion star.

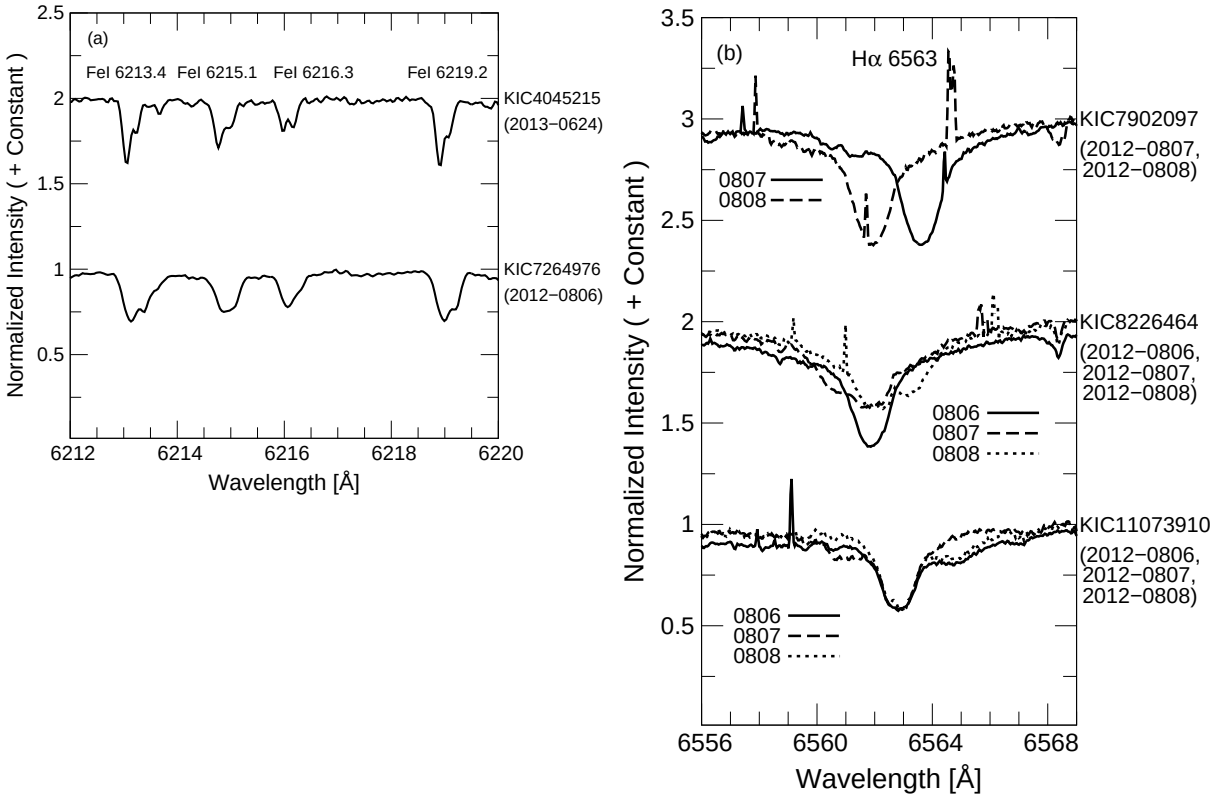

Fig. 2. Example of spectra of stars that we consider spectroscopic binary stars. The wavelength scale is adjusted to the heliocentric frame. Figures of all spectroscopic binary stars are shown in Supplementary Figure 2.

(a) Stars that show double-lined profiles. (b) Stars whose spectral lines show time variations between multiple observations, which are expected to be caused by the orbital motion in the binary system.

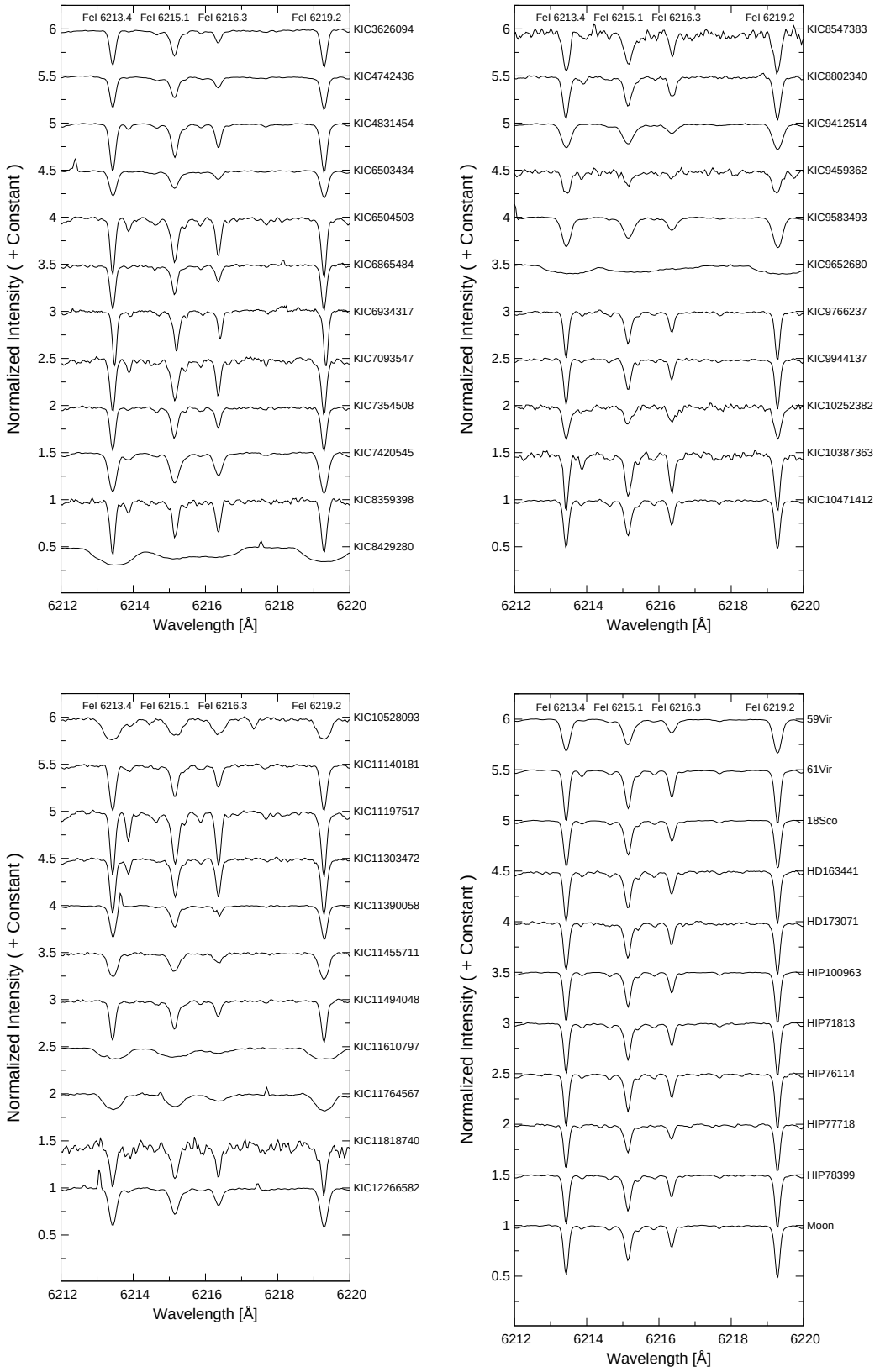

Fig. 3. Example of photospheric absorption lines, including Fe I 6213, 6215, 6216, and 6219, of 34 superflare stars that show no evidence of binarity, 10 comparison stars, and Moon. The wavelength scale is adjusted to the laboratory frame. Co-added spectra are used here in case that the star was observed multiple times.

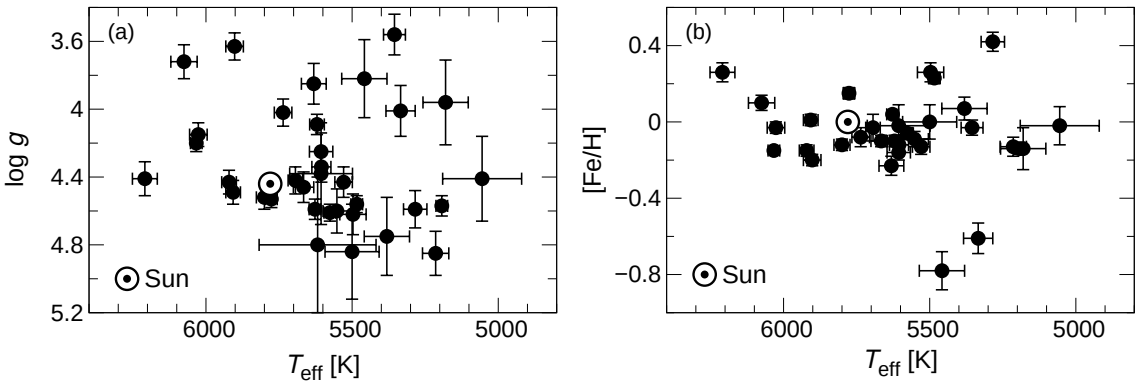

Fig. 4. Temperature ($T_{\rm eff}$), surface gravity ($\log g$), and metallicity ([Fe/H]) of the target superflare stars. These values are estimated by using our spectral data. The solar value is also plotted using a circled dot point.

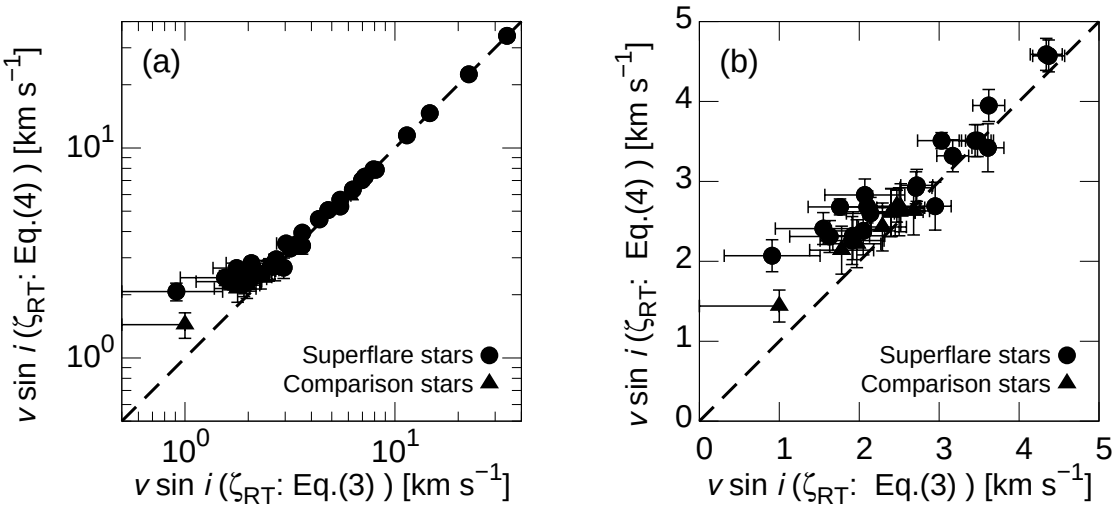
(a)
$v \sin i$ ($\zeta_{\rm RT}$: Eq.(4)) [km s^{-1}]
Superflare stars
Comparison stars
$v \sin i$ ($\zeta_{\rm RT}$: Eq.(3)) [km s^{-1}]
(b)
$v \sin i$ ($\zeta_{\rm RT}$: Eq.(4)) [km s^{-1}]
Superflare stars
Comparison stars
$v \sin i$ ($\zeta_{\rm RT}$: Eq.(3)) [km s^{-1}]

Fig. 5. (a) Comparison of two types of $v \sin i$ value using the other equations (Equation (3) and (4)) for the estimation of macroturblence velocity ($\zeta_{\rm RT}$) in the process of $v \sin i$ measurement. The black circles correspond to the data of our target superflare stars, while the black triangles are the data of comparison stars.

(b) Extended figure of (a). The plot range is limited to $0 \leq v \sin i \leq 5$ km s^{-1}.

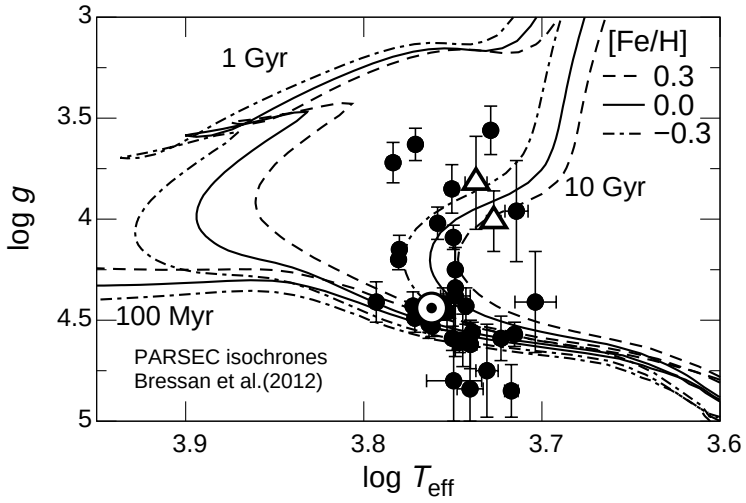

Fig. 6. Scatter plot of temperature ($T_{\rm eff}$) vs. surface gravity ($\log g$) of the target stars. Plotted values are estimated by using our spectral data. Two a bit "metal-poor" stars ([Fe/H]< -0.6) KIC 9459362 and KIC 10252382 among our target stars are plotted by using triangle points. The overplotted 6 lines show stellar age values of 1 and 10 Gyr for three different metallicity values ([Fe/H]$= 0.3, 0.0, -0.3$) on the basis of PARSEC isochrones in Bressan et al. (2012). The solar value is also plotted using a circled dot point.

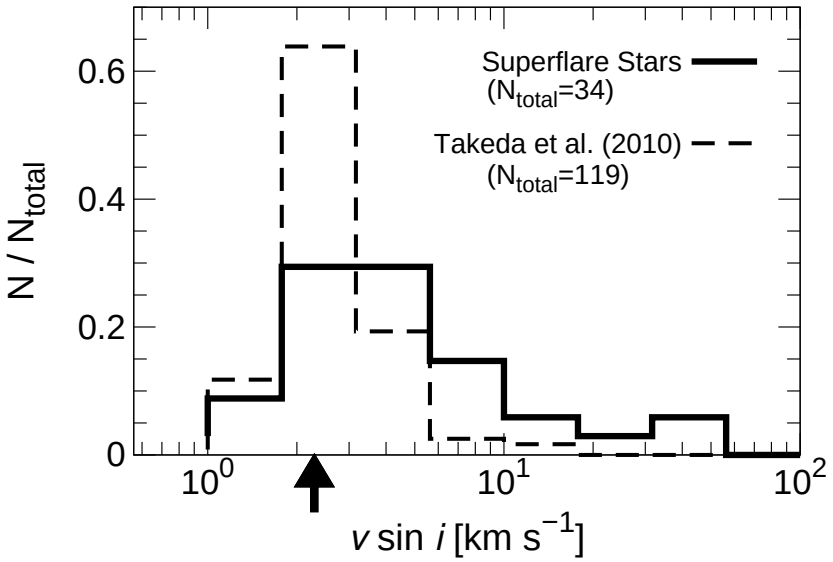

Fig. 7. Histograms showing the distribution of $v \sin i$. The filled line shows the data of superflare stars analyzed in this paper, while the dotted line shows those of ordinary solar-type stars reported in Takeda et al. (2010). The solar $v \sin i$ value is roughly indicated by a black upward arrow.

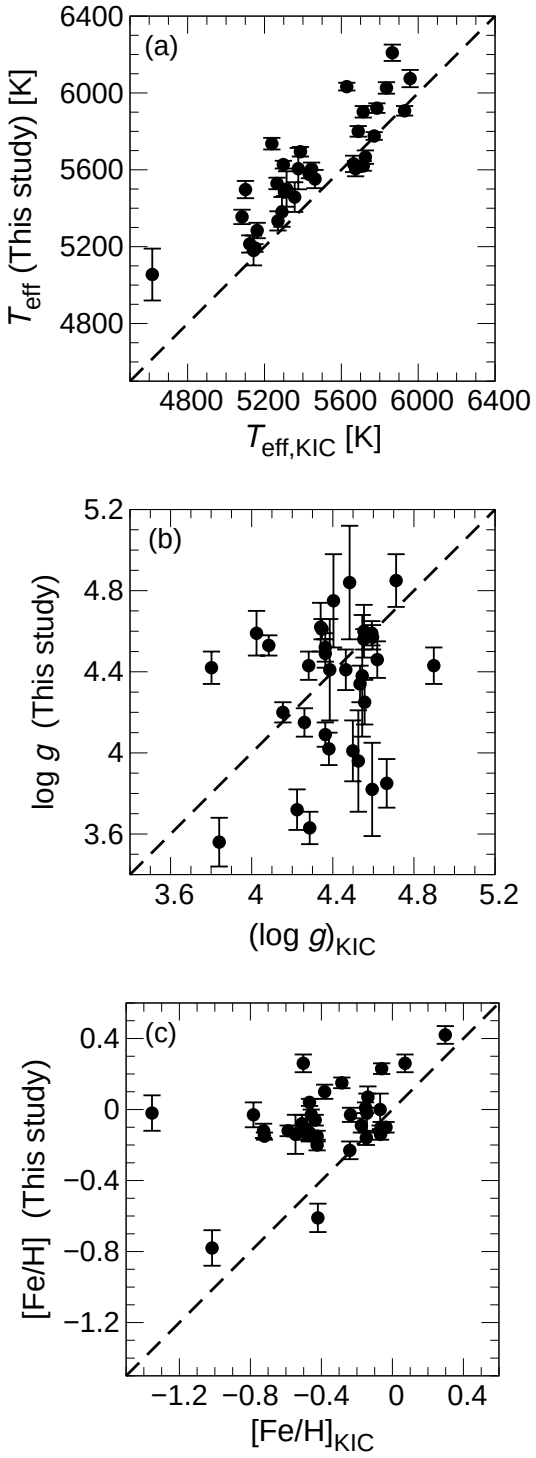

Fig. 8. Comparison between the atmospheric parameters ($T_{\rm eff}$, $\log g$, and [Fe/H]) that we estimate in this study, and those reported in the Kepler Input Catalog, respectively. The error bars indicate errors of the values in this study. KIC9652680 is not included here since the temperature value of KIC9652680 was not estimated from spectroscopic data as described in Section 3.2.

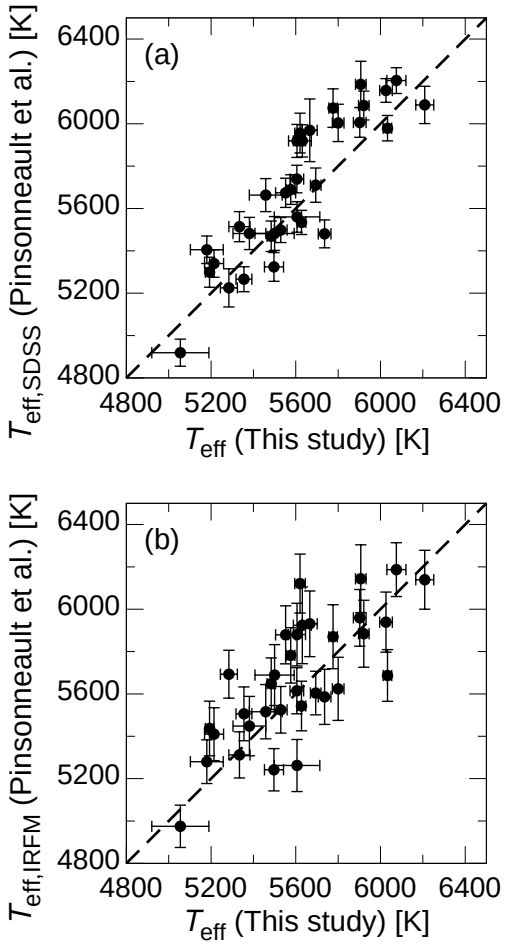

Fig. 9. Comparison of the temperature values in this study ($T_{\rm eff}$) with the value reported in Pinsonneault et al. (2012) ($T_{\rm eff,SDSS}$ and $T_{\rm eff,IRFM}$). KIC9652680 is not included here since we do not have the temperature value of KIC9652680 that was estimated from spectroscopic data as described in Section 3.2.

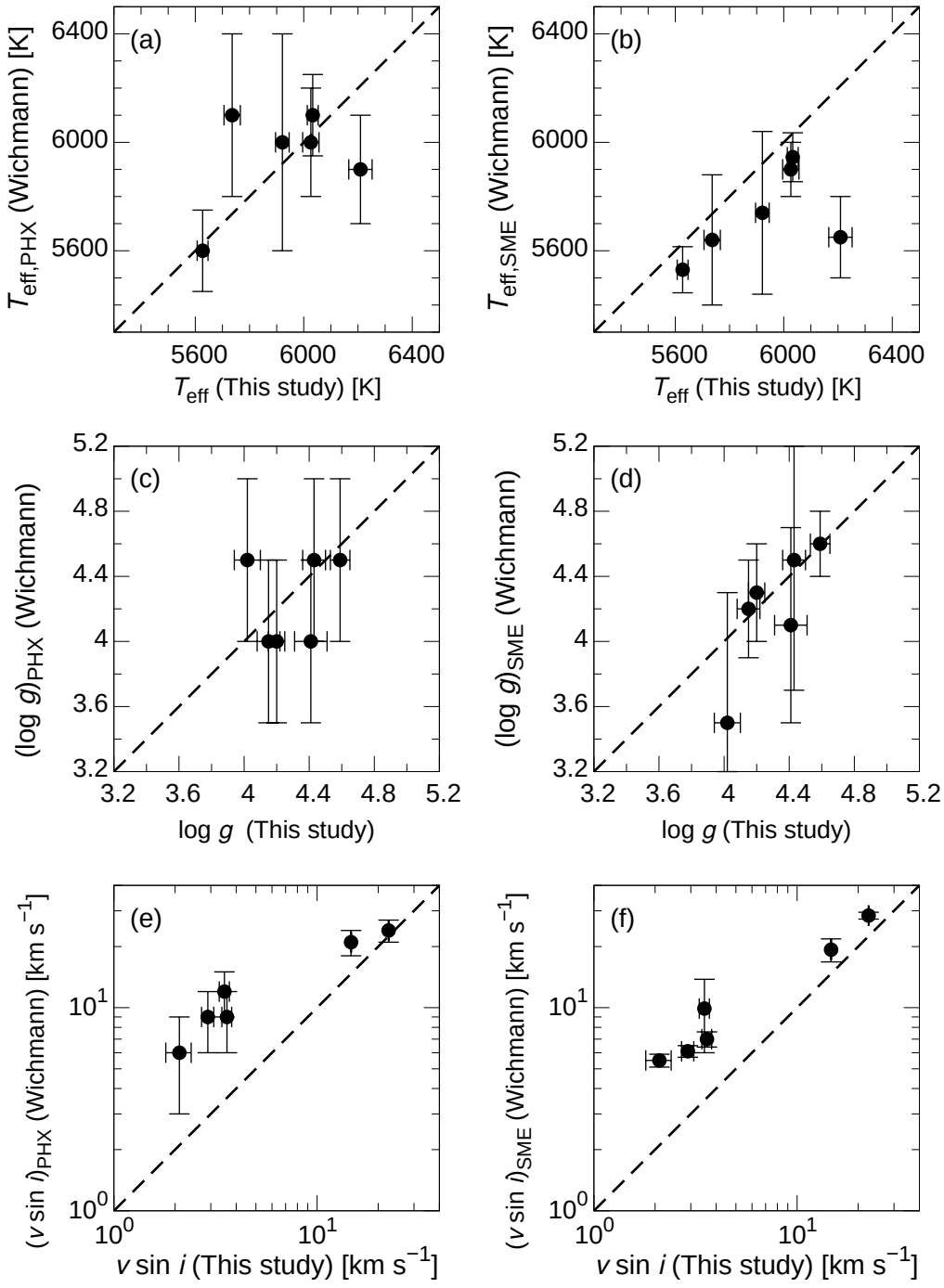

Fig. 10. Comparison of the temperature, surface gravity, and projected rotational velocity ($T_{\rm eff}$, $\log g$, and $v \sin i$) in this paper with those reported in Table 3 of Wichmann et al. (2014).

Table 1. Targets of our observations and their stellar parameters reported in the Online Data of Shibayama et al. (2013)[a].

Starname	binary[b]	$T_{\rm eff,KIC}$[c] [K]	$(\log g)_{\rm KIC}$[d] [cm s^{-2}]	$R_{\rm KIC}$[e] [$R_\odot$]	$K_p$mag[f] [mag]	$P_{\rm S}$[g] [day]	$(\rm BVAmp)_{\rm LF}$[h] [%]	Max $E_{\rm flare}$[i] [erg]
KIC3626094	no	5835	4.3	1.3	11.1	0.7	0.12	1.4×10^{35}
KIC4742436	no	5628	4.2	1.5	10.6	2.3	0.28	2.0×10^{35}
KIC4831454	no	5298	4.6	0.8	10.7	5.2	2.80	2.8×10^{34}
KIC6503434	no	5714	4.3	1.2	12.6	3.9	0.21	7.5×10^{34}
KIC6504503	no	5304	4.6	0.9	12.8	30.5	0.13	4.3×10^{33}
KIC6865484	no	5688	4.4	1.1	13.8	11.2	0.68	9.9×10^{34}
KIC6934317[j]	no	5387	3.8	2.3	12.3	2.5[a]	0.10[a]	8.4×10^{35}[a]
KIC7093547	no	5101	4.3	1.1	13.8	14.3	0.13	1.4×10^{34}
KIC7354508	no	5714	4.4	1.1	13.4	17.0	0.80	7.7×10^{33}
KIC7420545	no	5083	3.8	2.2	10.0	36.2[a]	1.13[a]	3.3×10^{35}[a]
KIC8359398	no	5123	4.7	0.7	14.1	13.5	1.66	3.1×10^{34}
KIC8429280	no	4616	4.4	1.0	9.6	0.6[a]	3.52[a]	9.1×10^{34}[a]
KIC8547383	no	5376	4.5	0.9	14.2	14.8	0.76	1.5×10^{35}
KIC8802340	no	5265	4.9	0.6	13.0	10.6	1.95	6.6×10^{33}
KIC9412514	no	5958	4.2	1.4	11.4	3.7	0.03	8.6×10^{33}
KIC9459362	no	5357	4.6	0.8	14.1	12.3	1.46	1.0×10^{35}
KIC9583493	no	5445	4.5	0.9	12.7	5.3	1.48	5.6×10^{34}
KIC9652680	no	5618	4.8	0.7	11.2	1.4	4.54	4.1×10^{34}
KIC9766237[j]	no	5674	4.6	0.9	13.9	21.8	0.14	1.1×10^{34}
KIC9944137[j]	no	5725	4.6	0.8	13.8	25.3	0.05	9.9×10^{33}
KIC10252382	no	5270	4.5	0.9	14.0	17.8	2.57	5.5×10^{34}
KIC10387363	no	5291	4.4	1.0	14.2	27.4	0.27	1.6×10^{34}
KIC10471412	no	5771	4.1	1.6	13.4	15.1	0.20	5.2×10^{35}
KIC10528093	no	5143	4.5	0.9	13.6	12.5	2.56	1.7×10^{35}
KIC11140181	no	5463	4.6	0.9	13.3	11.2	1.32	1.5×10^{34}
KIC11197517	no	5162	4.0	1.7	12.6	19.1	0.29	1.1×10^{34}
KIC11303472	no	5150	4.6	0.8	13.7	13.8	1.67	5.7×10^{33}
KIC11390058	no	5785	4.3	1.3	12.6	12.1	0.47	1.7×10^{34}
KIC11455711	no	5664	4.7	0.8	14.0	13.9	1.74	1.0×10^{34}
KIC11494048	no	5929	4.4	1.1	13.4	14.9	0.42	2.8×10^{34}
KIC11610797	no	5865	4.5	1.0	11.5	1.6	2.47	3.5×10^{35}
KIC11764567	no	5238	4.4	1.1	13.2	22.2	1.90	1.1×10^{35}
KIC11818740	no	5315	4.5	0.9	14.2	15.2	1.35	3.3×10^{34}
KIC12266582	no	5434	4.3	1.1	13.0	6.8	1.21	4.0×10^{34}

Table 1. (Continued)

Starname	binary[b]	$T_{\rm eff,KIC}$[c] [K]	$(\log g)_{\rm KIC}$[d] [cm s^{-2}]	$R_{\rm KIC}$[e] [$R_\odot$]	$K_p$mag[f] [mag]	$P_{\rm S}$[g] [day]	$(\rm BVAmp)_{\rm LF}$[h] [%]	Max $E_{\rm flare}$[i] [erg]
KIC7902097	yes (RV)	5626	4.6	0.8	12.3	3.9	0.88	1.3×10^{34}
KIC8226464	yes (Hα-vari)	5754	4.1	1.7	11.5	3.1	1.55	5.3×10^{35}
KIC11073910	yes (Hα-vari)	5381	4.6	0.8	11.7	2.1	1.12	3.2×10^{34}
KIC4045215	yes (SB2)	5229	4.5	1.0	13.6	12.0	0.12	1.8×10^{34}
KIC5445334	yes (SB2)	5137	4.7	0.7	12.8	7.7	0.55	1.6×10^{34}
KIC7264976	yes (SB2)	5184	4.1	1.7	12.0	12.6	3.08	9.8×10^{35}
KIC8479655	yes (SB2)	5126	4.6	0.8	12.8	19.3	3.09	3.8×10^{35}
KIC9653110	yes (SB2)	5223	4.4	1.0	12.9	1.6	3.27	7.4×10^{34}
KIC9764192	yes (SB2)	5551	4.6	0.8	12.9	3.5	2.76	3.2×10^{34}
KIC9764489	yes (SB2)	5447	4.7	0.7	14.1	10.7	2.25	8.7×10^{33}
KIC10120296	yes (SB2)	5490	4.4	1.1	12.9	3.9	1.83	1.1×10^{36}
KIC10453475	yes (SB2)	5202	4.5	1.0	14.2	15.2	5.59	6.4×10^{35}
KIC4138557	yes (VB)	5675	4.5	1.0	12.0	1.0	0.34	5.4×10^{34}
KIC4750938	yes (VB)	5804	4.3	1.2	12.9	2.1	1.19	9.8×10^{34}
KIC5896387	yes (VB)	5560	4.4	1.1	13.2	11.3	0.43	1.1×10^{35}
KIC11560431	yes (VB)	5094	4.5	0.9	9.7	3.1 [a]	1.80 [a]	6.1×10^{34} [a]

[a] KIC7420545, KIC6934317, KIC8429280, and KIC11560431 are not reported in Shibayama et al. (2013) since they are not solar-type stars on the basis of KIC parameters, as mentioned in Section 2.1. We newly analyzed the Kepler photometric data of these stars in the same way as in Shibayama et al. (2013).

[b] For the details of this column, see Section3.1. "no" means that the star show no evidence of binary system. "yes (SB2)" correspond to stars that have double-lined profile. "yes (RV)" means that the star show radial velocity changes, while "yes (Hα-vari)" correspond to stars whose Hα line profile show changes between the multiple observations. In addition, "yes (VB)" means that the star has a visual companion star.

[c] Effective temperature reported in Kepler Input Catalog (KIC; Brown et al. 2011).

[d] Surface gravity reported in KIC.

[e] Stellar radius in units of solar radius, which is reported in KIC.

[f] Kepler band magnitude in KIC.

[g] Period of the stellar brightness variation calculated in Shibayama et al. (2013) from the Kepler Q0∼6 data.

[h] Amplitude of the stellar brightness variation (%). The amplitude values listed here are estimated using Kepler data of the specific Quarter in which the largest superflare event of each star is detected. (The amplitude values estimated from the data of each Quarter are listed in the Supplementary Data of Paper II.)

[i] Energy of the largest superflare event of each star reported in Shibayama et al. (2013).

[j] We have already reported the results of our spectroscopic observation of KIC6934317 in Notsu et al. (2013a), and those of KIC9766237 and KIC9944137 in Nogami et al. (2014), respectively.

Table 2. Target superflare stars that can be identified with the ROSAT X-ray source.

Starname	ROSAT ID	count rate [s^{-1}]	position error [arcsec]
KIC4742436	1RXS J192149.3+395017	0.0122±0.0063	14
KIC4831454	1RXS J192200.0+395957	0.0166±0.0070	17
KIC8429280	1RXS J192502.2+442948	0.2423±0.0218	8
KIC11610797	1RXS J192737.8+493949	0.0186±0.0063	27
KIC11560431	1RXS J193016.8+493156	0.1660±0.0153	9

Table 3. Number of the single and binary stars. [a]

–	Single	Binary [b]	Sum.
$P_0 \geq 20$day	4	0	4
$10 \leq P_0 < 20$day	19	5	24
$P_0 < 10$day	11	11(4)	22
Sum.	34	16(4)	50
$P_S \geq 20$day	6	0	6
$10 \leq P_S < 20$day	17	6(1)	23
$P_S < 10$day	11	10(3)	21
Sum.	34	16(4)	50

[a] The values of P_0 and P_S are listed in Supplementary Table 1.

[b] Numbers in parentheses correspond to visual binary stars.

Table 4. Stellar paremeters of the superflare stars estimated from our spectroscopic results.

Starname	$v \sin i$ [km s^{-1}]	$T_{\rm eff}$ [K]	$\log g$ [cm s^{-2}]	$v_{\rm t}$ [km s^{-1}]	[Fe/H]	$R_{\rm s}$ [a, b] [$R_\odot$]	P_0 [c] [days]
KIC3626094	2.9 ± 0.2	6026 ± 30	4.15 ± 0.07	1.17 ± 0.12	-0.03 ± 0.03	1.44 ± 0.13	0.7
KIC4742436	3.6 ± 0.2	6033 ± 20	4.20 ± 0.05	1.09 ± 0.17	-0.15 ± 0.02	1.31 ± 0.08	2.3
KIC4831454	2.1 ± 0.3	5627 ± 20	4.59 ± 0.06	1.13 ± 0.10	0.04 ± 0.02	0.88 ± 0.01	5.2
KIC6503434	5.5 ± 0.1	5902 ± 30	3.63 ± 0.08	0.96 ± 0.13	-0.20 ± 0.03	3.01 ± 0.13	3.9
KIC6504503	1.6 ± 0.5	5484 ± 20	4.56 ± 0.05	0.77 ± 0.16	0.23 ± 0.03	0.90 ± 0.02	31.8
KIC6865484	2.7 ± 0.2	5800 ± 28	4.52 ± 0.07	1.11 ± 0.13	-0.12 ± 0.03	0.91 ± 0.04	10.3
KIC6934317	1.9 ± 0.4 [d]	5694 ± 25 [d]	4.42 ± 0.08 [d]	0.87 ± 0.14 [d]	-0.03 ± 0.07 [d]	0.99 ± 0.08	2.5
KIC7093547	2.1 ± 0.4	5497 ± 45	4.62 ± 0.12	0.18 ± 0.44	0.26 ± 0.05	0.91 ± 0.02	14.2
KIC7354508	3.2 ± 0.2	5620 ± 25	4.09 ± 0.06	0.92 ± 0.11	-0.10 ± 0.03	1.48 ± 0.02	16.8
KIC7420545	6.3 ± 0.2	5355 ± 38	3.56 ± 0.12	1.30 ± 0.14	-0.03 ± 0.04	3.45 ± 0.58	36.2
KIC8359398	1.8 ± 0.4	5214 ± 45	4.85 ± 0.13	0.75 ± 0.40	-0.13 ± 0.05	0.73 ± 0.02 [b]	12.7
KIC8429280	37.1 ± 3 [e]	5055 ± 135 [e]	4.41 ± 0.25 [e]	–	-0.02 ± 0.10 [e]	0.76 ± 0.06	1.2
KIC8547383	4.4 ± 0.2	5606 ± 108	4.38 ± 0.30	0.83 ± 0.35	-0.02 ± 0.11	1.16 ± 0.33	14.8
KIC8802340	4.3 ± 0.2	5529 ± 30	4.43 ± 0.09	1.25 ± 0.18	-0.13 ± 0.04	0.89 ± 0.05	10.3
KIC9412514	8.1 ± 0.1	6075 ± 45	3.72 ± 0.10	1.55 ± 0.16	0.10 ± 0.04	2.85 ± 0.38	3.7
KIC9459362	7.0 ± 0.1	5458 ± 78	3.82 ± 0.23	1.39 ± 0.47	-0.78 ± 0.10	2.31 ± 0.28	12.6
KIC9583493	7.2 ± 0.1	5605 ± 33	4.34 ± 0.09	1.28 ± 0.18	-0.12 ± 0.04	0.98 ± 0.04	5.5
KIC9652680	34.2 ± 0.1 [f]	5618 ± 200 [f]	4.80 ± 0.40 [f]	1 [f]	-0.30 [f]	0.84 ± 0.12	1.5
KIC9766237	2.1 ± 0.4 [g]	5606 ± 40 [g]	4.25 ± 0.11 [g]	0.88 ± 0.17 [g]	-0.16 ± 0.04 [g]	1.19 ± 0.31 [b]	14.2
KIC9944137	1.9 ± 0.4 [g]	5666 ± 35 [g]	4.46 ± 0.09 [g]	0.93 ± 0.13 [g]	-0.10 ± 0.03 [g]	0.93 ± 0.09	12.6
KIC10252382	5.5 ± 0.2	5334 ± 50	4.01 ± 0.15	1.40 ± 0.42	-0.61 ± 0.08	2.04 ± 0.11 [b]	16.8
KIC10387363	1.5 ± 0.6	5381 ± 78	4.75 ± 0.23	0.65 ± 0.39	0.07 ± 0.06	0.84 ± 0.03	29.9
KIC10471412	2.7 ± 0.2	5776 ± 20	4.53 ± 0.05	0.91 ± 0.15	0.15 ± 0.03	0.97 ± 0.02	15.2
KIC10528093	11.4 ± 0.1	5180 ± 78	3.96 ± 0.25	0.71 ± 0.44	-0.14 ± 0.11	2.06 ± 0.30	12.2
KIC11140181	3.6 ± 0.2	5552 ± 48	4.60 ± 0.13	1.25 ± 0.16	-0.09 ± 0.04	0.85 ± 0.05	11.5
KIC11197517	0.9 ± 0.6	5284 ± 40	4.59 ± 0.11	0.62 ± 0.35	0.42 ± 0.05	0.90 ± 0.04	14.3
KIC11303472	2.1 ± 0.5	5193 ± 20	4.57 ± 0.06	0.93 ± 0.16	-0.14 ± 0.03	0.76 ± 0.04	13.5
KIC11390058	3.5 ± 0.2	5921 ± 25	4.43 ± 0.07	1.11 ± 0.13	-0.15 ± 0.03	1.00 ± 0.08	12.0
KIC11455711	7.9 ± 0.1	5631 ± 43	3.85 ± 0.12	1.16 ± 0.14	-0.23 ± 0.05	2.09 ± 0.38	13.9
KIC11494048	3.4 ± 0.2	5907 ± 25	4.49 ± 0.07	1.03 ± 0.17	0.01 ± 0.03	0.98 ± 0.05	14.8
KIC11610797	22.5 ± 0.1	6209 ± 43	4.41 ± 0.10	1.70 ± 0.20	0.26 ± 0.05	1.23 ± 0.07	1.6
KIC11764567	14.7 ± 0.1	5736 ± 30	4.02 ± 0.08	1.71 ± 0.26	-0.08 ± 0.05	1.60 ± 0.16	22.4
KIC11818740	3.0 ± 0.3	5500 ± 93	4.84 ± 0.28	0.80 ± 0.47	0.00 ± 0.09	0.83 ± 0.02	15.4

Table 4. (Continued)

Starname	$v \sin i$ [km s^{-1}]	$T_{\rm eff}$ [K]	$\log g$ [cm s^{-2}]	$v_{\rm t}$ [km s^{-1}]	[Fe/H]	$R_{\rm s}$ [a, b] [$R_\odot$]	P_0 [c] [days]
KIC12266582	4.8 ± 0.2	5576 ± 20	4.61 ± 0.05	1.20 ± 0.12	-0.06 ± 0.03	0.83 ± 0.01	6.9

[a] The resultant stellar radius ($R_{\rm s}$) value in this column is a median between the maximum and minimum values among all the possible $R_{\rm s}$ values selected from the isochrone data. The error value in this column corresponds to these maximum and minimum values.

[b] When we estimate $R_{\rm s}$ values, KIC8359398, KIC9766237, and KIC10252382 have no suitable isochrones within their original error range of $T_{\rm eff}$ and $\log g$. For these three stars, we then took into account $2\Delta T_{\rm eff}$ and $2\Delta \log g$. We must note that the resultant values of these three stars can have relatively low accuracy.

[c] Period value estimated from the Kepler Quarter 2∼16 data, which is explained in Section 2.1.

[d] We already reported the values of KIC6934317 in Notsu et al. (2013a).

[e] We list the values of KIC8429280 reported in Frasca et al. (2011) since the rotational velocity is so high and the spectral lines are too wide to estimate atmosphric parameters ($T_{\rm eff}$, $\log g$, and [Fe/H]) in our way using equivalent width of Fe I/II lines (See Section 3.2 for the details).

[f] KIC values are listed and used for investigating $v \sin i$ and $R_{\rm s}$ since the rotational velocity of KIC9652680 is so high and the spectral lines of these stars are too wide to estimate atmosphric parameters ($T_{\rm eff}$, $\log g$, and [Fe/H]) in our way using equivalent width of Fe I/II lines (See Section 3.2 for the details). Microturbulence velocity ($v_{\rm t}$) is assumed to be 1 km s^{-1} when we estimated $v \sin i$.

[g] We already reported the values of KIC9766237 and KIC9944137 in Nogami et al. (2014).

Appendix 1. Comparison of period values

Two period values (P_S and P_1), which are explained in Section 2.1, are listed in Supplementary Table 1. We also listed other period values P_2 and P_3, which correspond to the second and third peak of the power spectra used for estimating P_1, respectively. We compare the above two period value ($P_{\rm S}$ and P_1) in Figure 11 (a). Figure 11 (a) shows that P_1 is not so well consistent with $P_{\rm S}$ for longer period values ($P > 15$ days), but, in such cases, P_2 or P_3 are well consistent with $P_{\rm S}$. We can also see two clear branches in the plotted distribution of the data points in Figure 11 (a). These two branches correspond to $P_{\rm S} \approx P_{1,2,3}$ and $P_{\rm S} \approx (1/2)P_{1,2,3}$, respectively. The latter branch implies that half periods are sometimes selected when we use Kepler data (Q2$\sim$16 data; $\sim$1500 days) longer than those in Shibayama et al. (2013) (Q0$\sim$6 data; $\sim$500 days). We compared these period values, and checked by eye the lightcurves and power spectra shown in Supplementary Figure 1. We then selected the resultant period value P_0 from the above three period values (P_1, P_2 and P_3) by checking the lightcurve and power spectrum of each star by eye. The selection criteria are described in Section 2.1. In many cases, we adopt P_1 as P_0. The resultant P_0 values are listed in Supplementary Table 1 and plotted in Figure 11 (b). In Paper II, we use only P_0 as the period of the brightness variation, as explained in Section 2.1.

We also listed other period values ($P_{\rm R1}$, $P_{\rm R2}$, $P_{\rm N}$, and $P_{\rm M}$) in Supplementary Table 1 for comparison. $P_{\rm R1}$ and $P_{\rm R2}$ values are reported by Reinhold et al. (2013), and they only used Kepler Quarter 3 data ($\sim$90 days) for estimating their period values. According to Reinhold et al. (2013), $P_{\rm R1}$ correspond to their "primary" period value, while $P_{\rm R2}$ are their "second" period value, which they used for investigating the surface differential rotation. $P_{\rm N}$ values are reported in Nielsen et al. (2013), and they are derived from Kepler Quarter 2-9 data. $P_{\rm M}$ values are reported in McQuillan et al. (2014), and they are derived from Kepler Quarter 3-14 data. We compare these period values ($P_{\rm R1,R2}$, $P_{\rm N}$, and $P_{\rm M}$) with our resultant values (P_0) in Figures 12 (a), (b), and (c), respectively. These figures show that our resultant period values (P_0) and the above other period values ($P_{\rm R1,R2}$, $P_{\rm N}$, and $P_{\rm M}$) are consistent for most stars.

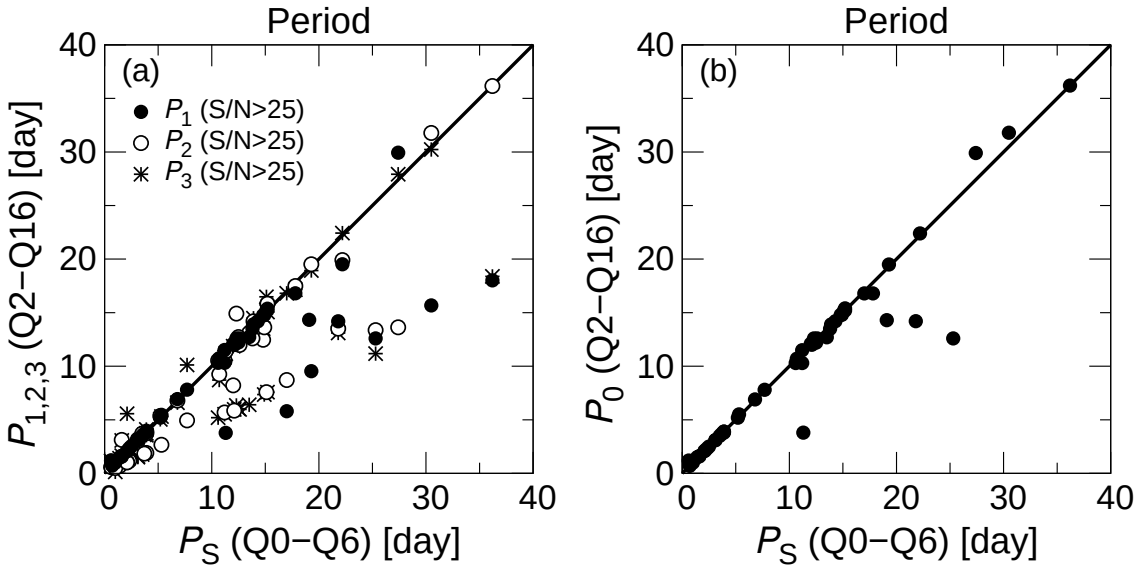

Fig. 11. (a) Comparison of the period value we newly estimated using Kepler Quarter 2∼16 data (P_1) with that in Shibayama et al. (2013) using Kepler Quarter 0∼6 data (P_S). In addition to P_1, the P_2 and P_3 values, which are the second and third peak of the power spectra of each star, are also plotted as a function of P_S. (b) Comparison of the resultant period value P_0 selected from P_1, P_2 and P_3 with that in Shibayama et al. (2013) using Kepler Quarter 0∼6 data (P_S).

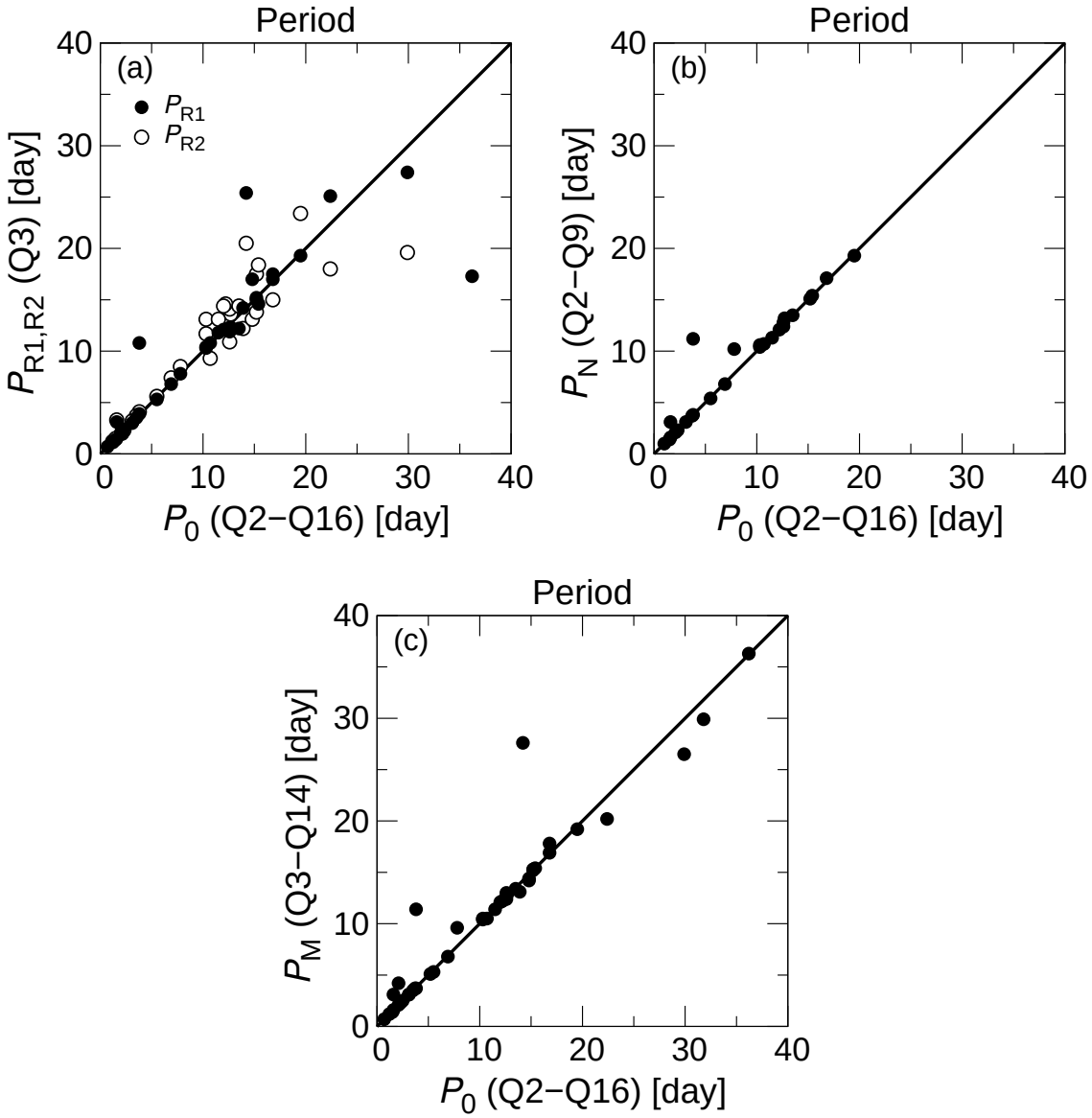

Fig. 12. (a) Comparison of our resultant period value P_0 estimated using Kepler Quarter 2∼16 data with the value estimated in Reinhold et al. (2013) using Kepler Quarter 3 data ($P_{\rm R1}$ and $P_{\rm R2}$). (b) Comparison of our resultant period value P_0 with the value estimated in Nielsen et al. (2013) using Kepler Quarter 2-9 data ($P_{\rm N}$). (c) Comparison of our resultant period value P_0 with the value estimated in McQuillan et al. (2014) using Kepler Quarter 3-14 data ($P_{\rm M}$).

Appendix 2. Lightcurves around the observational dates of S11B and S12B

We show the Kepler lightcurves obtained around the period of S11B and S12B observation in Figure 13. There are no lightcurve data for S13A observation since Kepler ended its general observation mode on 2013 May (Thompson et al. 2013d). No flare events were detected during the observation period.

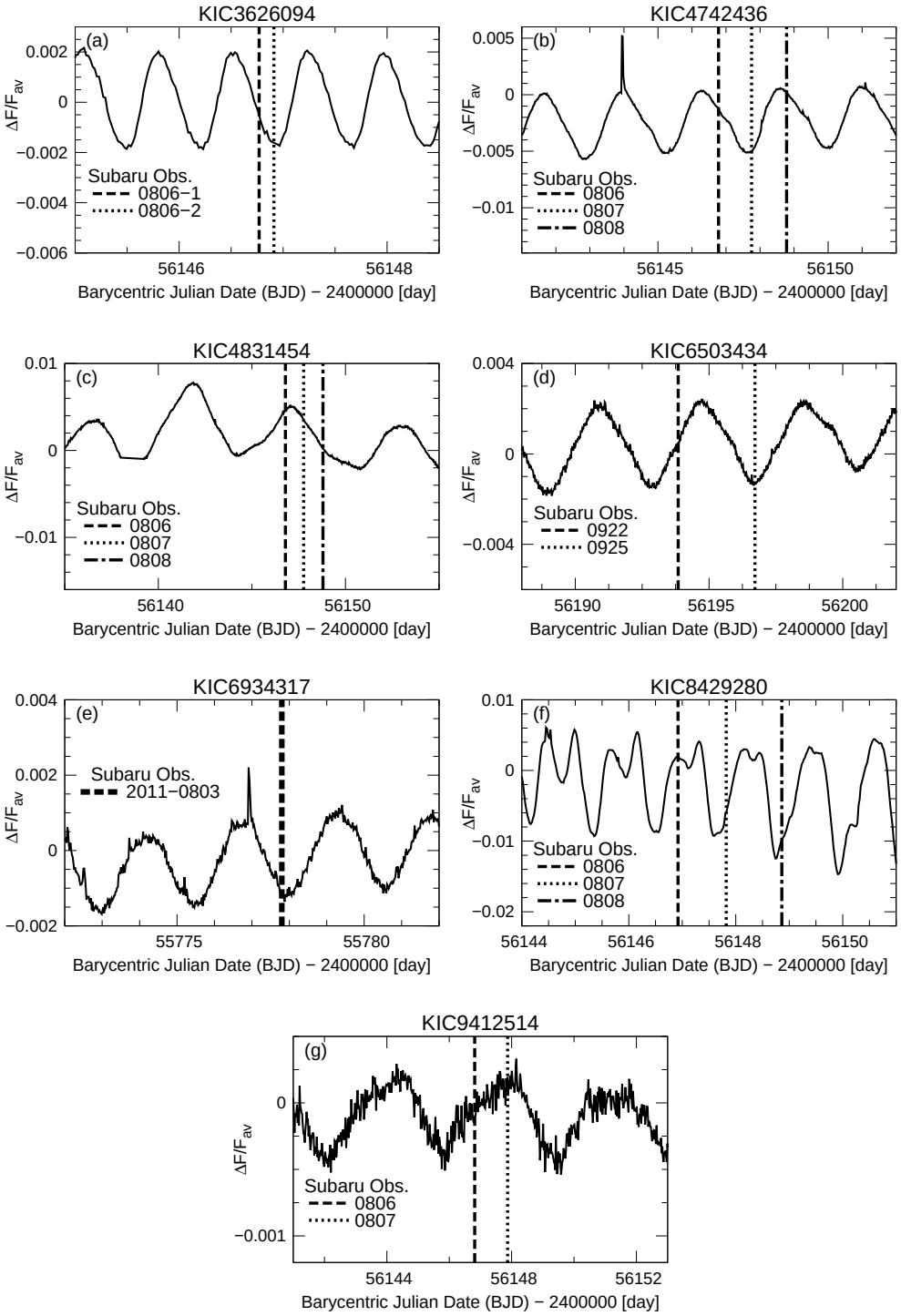

Fig. 13. Light curves of the target superflare stars around the observational dates of S11B (2011 August 3) and S12B (2012 August 6, 7, 8, and September 22, 23, 24, 25). Horizontal axes show Barycentric Julian Date, and vertical axes correspond to stellar brightness normalized by the average one ($F_{\rm av}$). Vertical dashed and dash-dotted lines show the observational date, respectively.

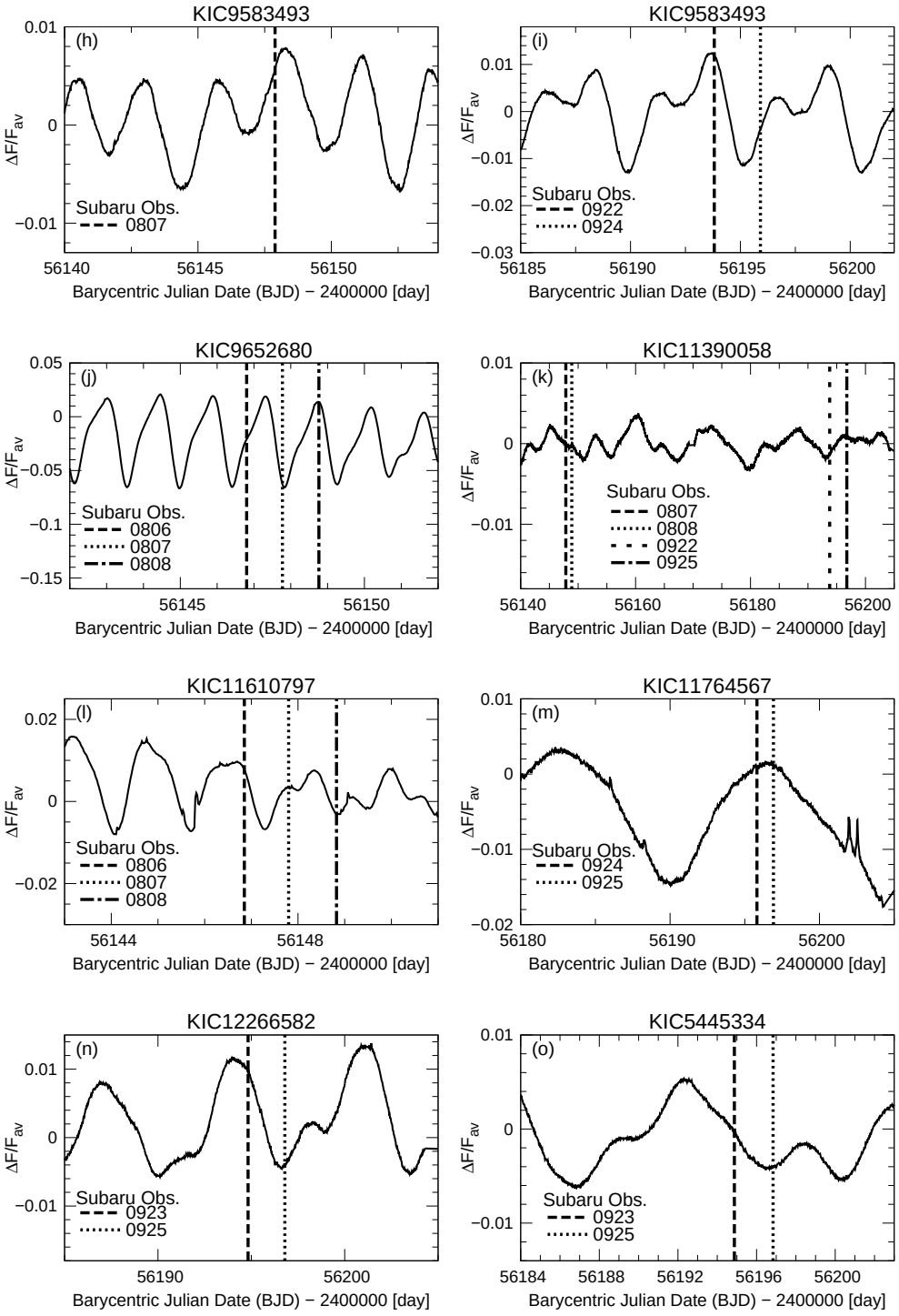

Fig. 13. Continued.

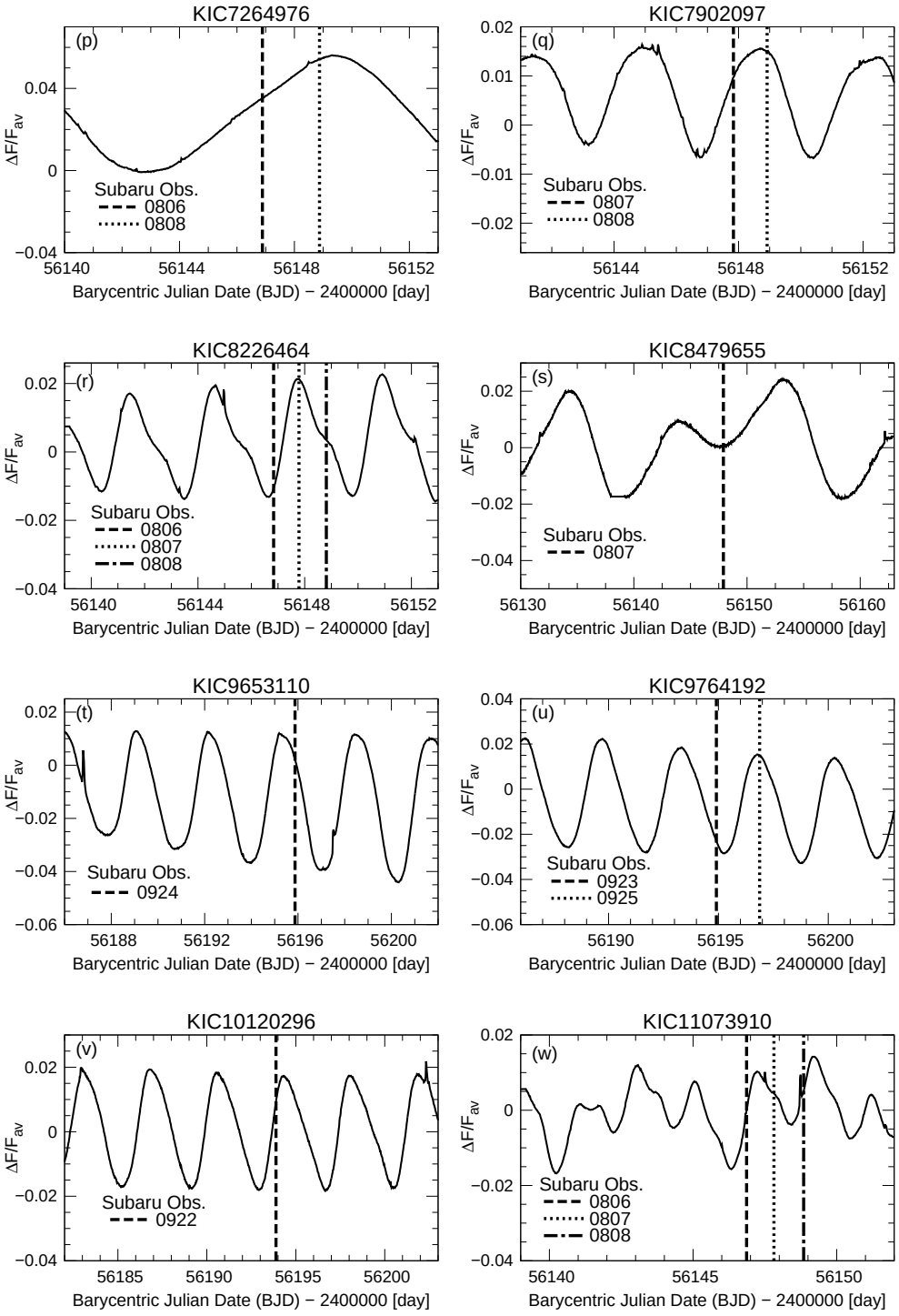

Fig. 13. Continued.

Appendix 3. Comparison stars

We estimated temperature ($T_{\rm eff}$), surface gravity ($\log g$), metallicity ([Fe/H]), projected rotational velocity ($v \sin i$), and stellar radius ($R_{\rm s}$) of 34 single superflare stars, 10 comparison stars, and Moon (Sun) in Section 3.2$\sim$3.4. The estimated values of 10 comparison stars and Moon (Sun) are listed in Table 5. The values reported by the previous studies were also listed in Table 5. In Figure 14, we compared our $T_{\rm eff}$, $\log g$, [Fe/H], and $v \sin i$ values of comparison stars including Moon with those reported by the previous studies listed in Table 5. Our values seem to be in good agreement with the previous values especially for $T_{\rm eff}$, [Fe/H], and $v \sin i$ values.

When estimating $v \sin i$ values, the choice of macroturbulence is often important, as we mentioned at the end of Section 4.3. We briefly summarize which formula was used for evaluating the macroturbulence velocity in the other studies whose $v \sin i$ values are listed in Table 5. Notsu et al. (2013a) (referred as (2) in Table 5) used the same formula as we do in this paper (Equation (3)). Anderson et al. (2010) (referred as (4)) treated the macroturbulence velocity as one of the free parameters in the process of spectral line fitting. Ammler-von Eiff & Reiners (2012) (referred as (5)) did not assume the macroturbulence velocity since they conducted line profile analyses in Fourier space (The detailed explanations are in the 8th paragraph of Section 1 of Ammler-von Eiff & Reiners (2012)). Takeda et al. (2010) (referred as (7)) assumed $v_{\rm mt} = 1.5$km s^{-1} since atmospheric parameters of most of their target stars are similar to the Sun. King et al. (2005) (refereed as (9)) did not consider the effect of macroturblence velocity and they could only estimate the upper limit of $v \sin i$.

Among the previous studies referred in Table 5, Takeda et al. (2005) and Takeda & Tajitsu (2009) used the basically same method for deriving $T_{\rm eff}$, $\log g$, and [Fe/H] of 59 Vir, 61 Vir, 18 Sco, HIP100963, and Moon as we have done in Section 3.2. In this method, equivalent width values of Fe I/II lines are used for deriving stellar parameters. Then, we here compared the measured equivalent width values (W_λ) of Fe I/II lines in this paper with those in Takeda et al. (2005) and Takeda & Tajitsu (2009). The results are shown in Figure 15. We can see that these two values are comparable, and that our measurement of equivalent width values are consistent with that of the previous studies.

Summarizing this section, we confirmed that our resultant atmospheric parameters and measured equivalent width values of comparison stars are comparable to the results of previous researches. We can say that our result of spectroscopic determination of atmospheric parameters is consistent with that of the previous studies.

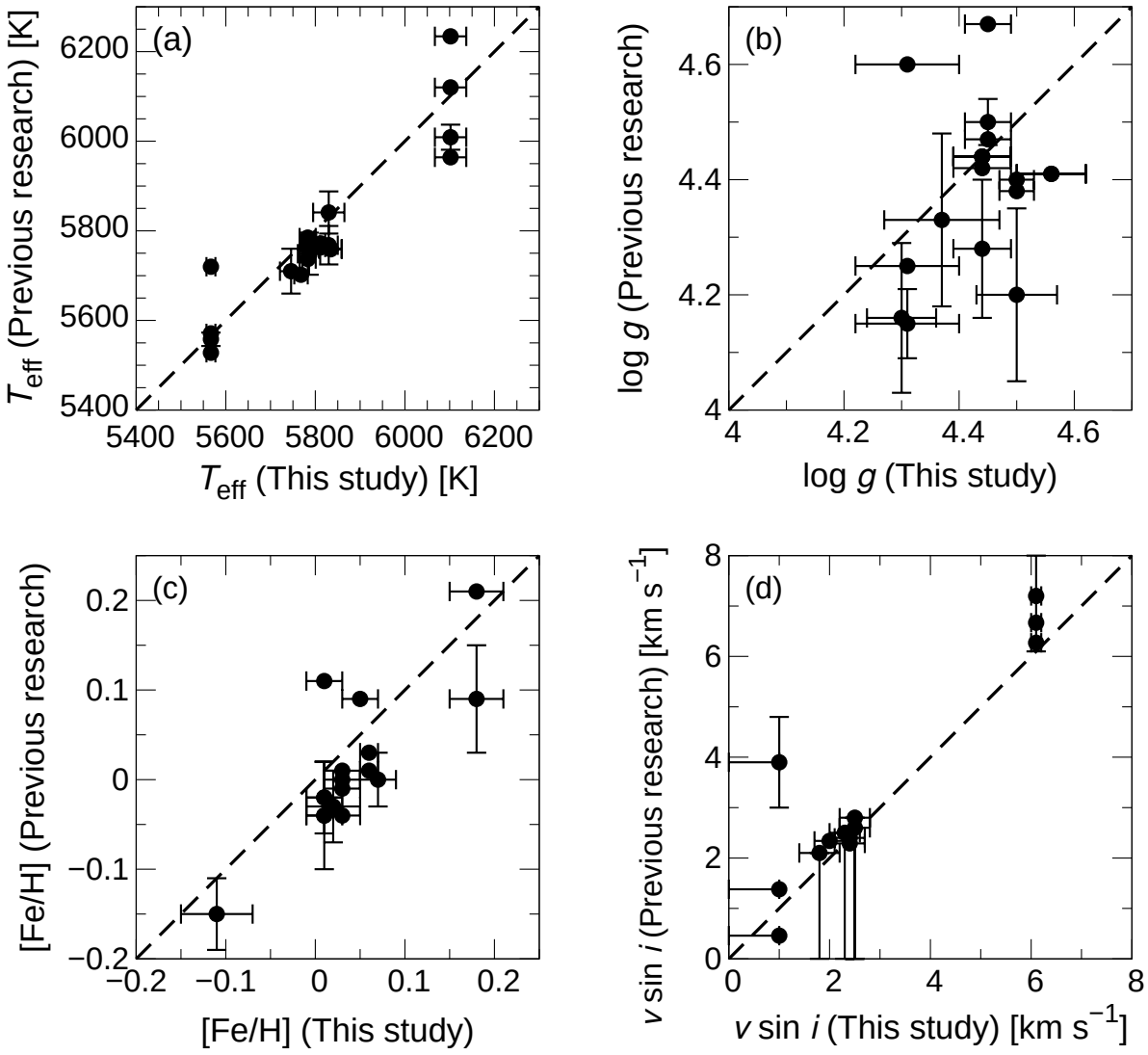

Fig. 14. Temperature ($T_{\rm eff}$), surface gravity ($\log g$), metallicity ([Fe/H]) and projected rotational velocity ($v \sin i$) of comparison stars including Moon, and comparison with previous results listed in Table 5.

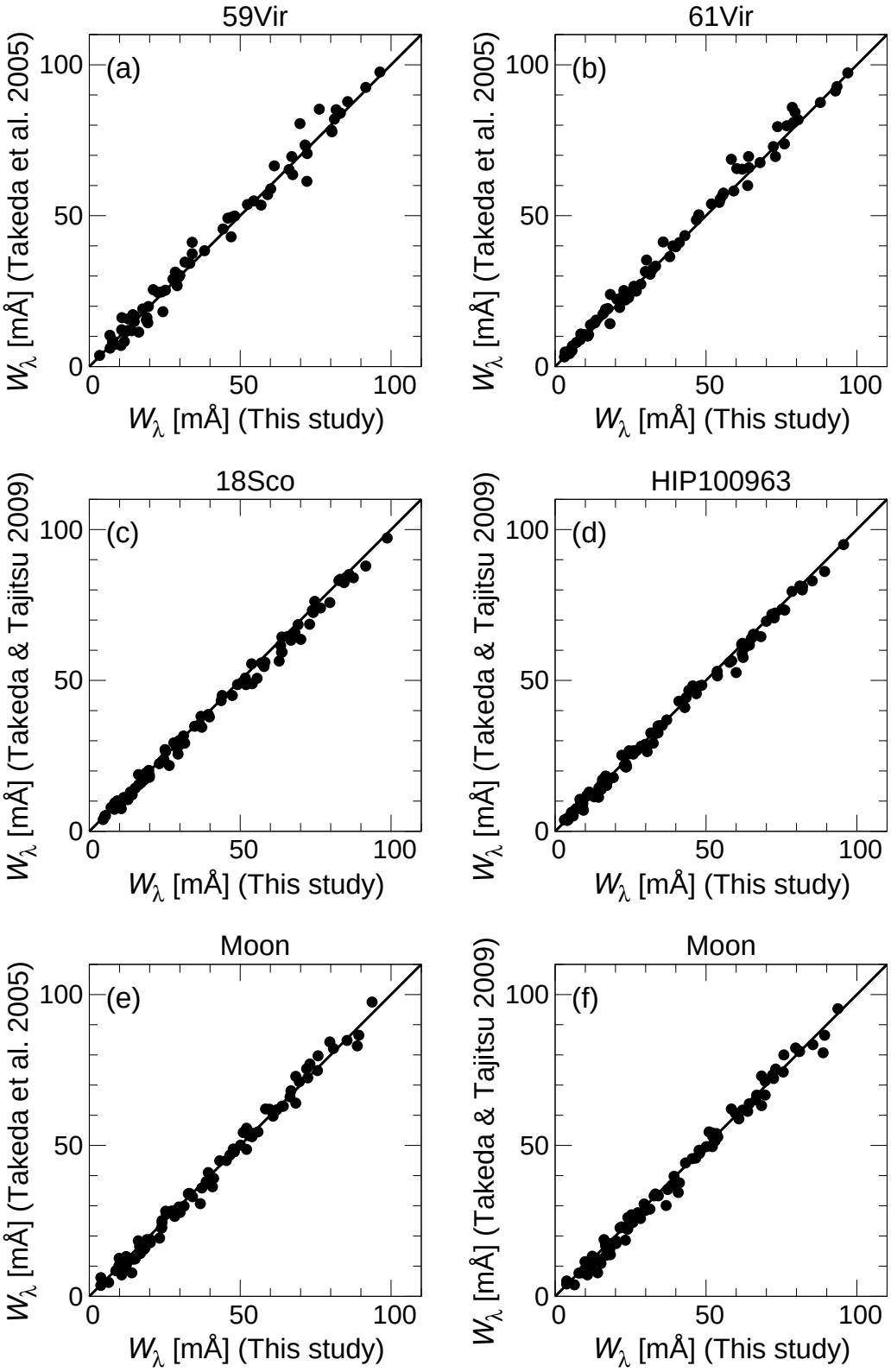

Fig. 15. Comparison of the EW values (W_λ) of Fe I and Fe II lines shown in Takeda et al. (2005) or Takeda & Tajitsu (2009) with those measured by us.

Table 5. Stellar parameters of comparison stars.

Starname	$v \sin i$	$T_{\rm eff}$	$\log g$	v_t	[Fe/H]	$M_{\rm s}$ [a]	$R_{\rm s}$ [b]	Ref. [c]
	[km s^{-1}]	[K]	[cm s^{-2}]	[km s^{-1}]		[$M_\odot$]	[$R_\odot$]	
59Vir	6.1± 0.1	6102± 35	4.31± 0.09	1.33± 0.14	0.18± 0.03	1.18± 0.03	1.27± 0.14	(1)
	6.27	6009± 28	4.15± 0.06	1.32± 0.09	0.09± 0.06			(2)
		6120	4.25		0.21	1.22		(3)
	6.67	6234	4.60					(4)
	7.2± 1.1	5964						(5)
61Vir	<1.0±	5567± 10	4.45± 0.04	0.87± 0.10	0.01± 0.02	0.90± 0.02	0.93± 0.03	(1)
	1.38	5558± 15	4.50± 0.04	0.87± 0.08	-0.04± 0.06			(2)
		5720	4.67		0.11	1.02		(3)
	0.46	5571	4.47					(4)
	3.9± 0.9	5528						(5)
18Sco	2.0± 0.3	5812± 10	4.50± 0.03	1.04± 0.08	0.06± 0.01	1.03± 0.01	0.96± 0.02	(1)
(HIP79672)		5772	4.40	0.97	0.01			(6)
	2.34	5763	4.38	0.97	0.03			(7)
HD163441	2.5± 0.3	5768± 15	4.45± 0.04	0.87± 0.11	0.05± 0.02	0.99± 0.02	0.98± 0.04	(1)
		5702			0.09			(8)
HD173071	2.7± 0.2	5982± 25	4.41± 0.07	0.98± 0.14	0.18± 0.03	1.13± 0.03	1.11± 0.07	(1)
		5875			-0.04			(8)
HIP100963	2.4± 0.3	5834± 25	4.56± 0.06	1.07± 0.09	0.01± 0.02	1.03± 0.02	0.93± 0.01	(1)
		5760	4.41	0.93	-0.04			(6)
	2.4	5759	4.41	0.98	-0.02			(7)
HIP71813	2.3± 0.3	5786± 25	4.30± 0.06	1.07± 0.09	0.01± 0.02	0.96± 0.02	1.15± 0.08	(1)
	<2.5	5749	4.16	1.22	-0.02			(9)
HIP76114	1.8± 0.4	5746± 25	4.50± 0.07	0.98± 0.11	0.02± 0.03	0.98± 0.03	0.94± 0.05	(1)
	<2.1	5710	4.20	1.35	-0.03			(9)
HIP77718	2.5± 0.3	5830± 35	4.37± 0.10	0.97± 0.17	-0.11± 0.04	0.93± 0.03	1.04± 0.11	(1)
	<2.8	5841	4.33	1.18	-0.15			(9)
HIP78399	2.5± 0.3	5830± 20	4.44± 0.05	1.04± 0.09	0.07± 0.02	1.02± 0.03	1.02± 0.05	(1)
	<2.6	5768	4.28	1.32	0.00			(9)
Moon	2.4± 0.3	5783± 18	4.44± 0.05	0.85± 0.13	0.03± 0.02	0.99± 0.02	1.00± 0.05	(1)
(Sun)		5785	4.44	0.96	0.01	1.00		(3)
		5737	4.42	0.95	-0.04			(6)
	2.29	5761	4.44	1.00	-0.01			(7)
	<2.5	5777	4.44	1.25	0.00			(9)

[a] The resultant stellar mass ($M_{\rm s}$) value in this column is a median between the maximum and minimum values among all the possible $M_{\rm s}$ values selected from the isochrone data. The error value in this column corresponds to these maximum and minimum values.

[b] The resultant stellar radius ($R_{\rm s}$) value in this column is a median between the maximum and minimum values among all the possible $R_{\rm s}$ values selected from the isochrone data. The error value in this column corresponds to these maximum and minimum values.

[c] (1) Present work. (2)Notsu et al. (2013a); (3)Takeda et al. (2005); (4)Anderson et al. (2010);

(5)Ammler-von Eiff & Reiners (2012); (6)Takeda & Tajitsu (2009); (7)Takeda et al. (2010);

(8)Datson et al. (2012); (9)King et al. (2005).